4open 2023, **6**, 8

https://doi.org/10.1051/fopen/2023007

4 Open

Available online at:
www.4open-sciences.org

Special issue of 4open on Inorganic Nanoparticle Luminophore: Design and Application

REVIEW ARTICLE OPEN ACCESS

Post-synthetic modification of semiconductor nanoparticles can generate lanthanide luminophores and modulate the electronic properties of preformed nanoparticles

Saoni Rudra, Madhumita Bhar, and Prasun Mukherjee*

Centre for Research in Nanoscience and Nanotechnology, University of Calcutta, JD-2, Sector-III, Salt Lake, Kolkata 700106, West Bengal, India

Received 30 June 2022, Accepted 27 June 2023

Abstract – Post-synthetic modification of inorganic nanoparticles (NPs) provides a unique lesser synthetically demanding opportunity to access nanomaterials those are oftentimes not directly realizable by conventional synthetic routes. Trivalent lanthanide (Ln^{3+}) incorporated (doped) semiconductor NPs can benefit from individual properties of the NPs and Ln^{3+} moieties. This work summarizes key outcomes from experiments when (a) ZnS /CdS /CdSe NPs are post-synthetically treated with Ln^{3+} to generate ZnS/Ln or CdSe/Ln [Ln = Pr, Nd, Sm, Eu, Tb, Dy, Ho, Er, Tm, Yb] and CdS/Ln [Eu, Tb] NPs, (b) synthetically Tb^{3+} doped Zn(Tb)S NPs are post-synthetically modified with varying concentration of heavy metals like Pb^{2+}/Cd^{2+} to generate Zn(Tb)S/M [M = Pb, Cd] NPs, and (c) the pH of Zn(Tb)S NPs aqueous dispersion is varied post-synthetically. Key observations from these experiments include (a) incorporation of Ln in all the post-synthetically prepared CA/Ln NPs, with presence of host sensitized dopant emission in select cases that can be rationalized by a charge trapping mediated dopant emission sensitization processes, (b) existence of rich photophysics in the sub-stoichiometric reactant concentration ratio, and (c) identifying the alteration of surface capping ligand structure as an important variable to control the Ln^{3+} emission. In summary, these experimental observations provide an easy control of reaction conditions either to generate Ln^{3+} inorganic NP luminophores or to control their electronic properties by modulating either the NP's core or surface properties, and are of potential usefulness in various luminescence based applications.

Keywords: Semiconductor nanoparticles, Lanthanides, Post-synthetic modification, Doping, Luminescence.

Introduction

Inorganic nanoparticles (NPs) offer a wide range of potential in both fundamental and application perspective. Synthesizing them by conventional bottom-up approaches like hot injection, [1, 2] heating up, [3, 4] sol–gel solvothermal [5, 6] methods are known. These synthetic protocols are established to generate materials in quantum confined regime, thus availing various unique properties. Besides these conventional synthetic routes which are time consuming, a unique way to tune the properties of nanomaterials is to treat them post-synthetically. That is, modifying an inorganic NP by treating them following their synthesis. An extremely fascinating avenue to this front is demonstrated by Alivisatos and co-workers [7] in 2004, where these researchers discussed feasibility of cation exchange with the formation of Ag_2Se NPs by treating CdSe NPs with Ag^+ at room temperature. In this reaction the incoming Ag^+ and outgoing Cd^{2+} exchange their spatial positions without perturbing the anionic framework of the nanocrystal. Furthermore, by adding excess of Cd^{2+} and adjusting the chemical nature of the surface capping ligand a reverse cation exchange is found to be possible. This outstanding observation opened up a ground to access a wide range of nanomaterials those are oftentimes not directly realizable using conventional synthetic protocols. Additionally, these reactions are facile and generally performed at or near ambient conditions, reduce much synthetic efforts and time, and are cost effective, as various nanomaterials can be accessed from a single batch of initial reactant NP synthesis. These reactions furthermore provide an easy comparison of physico-chemical properties of the reactant and product NPs. Comparison of NP's properties from different synthesis face challenges due to inherent batch to batch inhomogeneity.

This outstanding observation by Alivisatos and co-workers triggered related efforts in various research laboratories. Some of the demonstrated cation exchange by post-synthetic modification reactions include formation

*Corresponding author: pmcrnn@caluniv.ac.in, pmukherjee12@gmail.com

of CdS–Ag_2S nanorods [8], CdS–Cu_2S nanorods with a different morphology than that of CdS–Ag_2S nanorods [9], CdSe/CdS → Cu_2Se/Cu_2S → PbSe/PbS nanorods, [10] III–V nanocrystals (InP, InAs, GaP, and GaAs) [11], CdSe (core) – CdS (pods) → CdSe (core) – CdS/Cu_2S (pods) → $Cu_{2-x}Se$ (core) – Cu_2S (pods) [12], CdSe → Cu_2Se → ZnSe with size, shape and crystal structure conservation of the nanocrystals [13], alloyed quaternary and quinary copper chalcogenide nanocrystals [14], $Cu_{2-x}Se$ → Cu_2SnSe_3 and SnSe by addition of Sn^{4+} and Sn^{2+} respectively [15], Cu_2Te → CdTe [16], partially and completely exchanged CdSe/Ag and Ag_2Se nanoplatelets [17], InAs → InAs/Cu, InAs/Ag, InAs/Au [18], CdSe → CdSe/Ag [19], and LnF_3 → $Ln'F_3$ with atomic number of Ln > Ln′ [20]. These studies clearly point on the robustness of using cation exchange reactions to access nanomaterials with suitable incoming and outgoing cation pairs of differing size and charge. Few review articles are currently available discussing various facets of cation exchange reactions, covering demonstrated reactions with mechanistic insights based on thermodynamic and kinetic considerations [21–26].

Another scenario may arise where the incoming – outgoing cation pairs do not take part in exchange, but somehow can still alter the properties of the nanomaterial by altering the NP's surface properties. Such examples are discussed in the examination of spectra of Zn(Mn)S and ZnS/Mn NPs by Murphy and co-workers [27], where these researchers reported a dramatic difference in photophysical outcome between these two assemblies. While the synthetically doped Zn(Mn)S NPs give rise to blue ZnS centered and orange Mn^{2+} centered emissions, the ZnS/Mn NPs yield a blue shifted ZnS emission without Mn^{2+} signal. Similarly, Chrysochoos and co-workers [28] discussed modulation of CdS NP's surface properties by addition of Cu^{2+} post-synthetically. Collectively, post-synthetic modification of inorganic NPs with a suitable cation pair can result in cation exchange, and even when this is absent mere alteration of NP's surface state composition may also be able to access modified properties.

Doping an inorganic NP has the ability to tune the chemical, optical, magnetic, electrical, electronic properties; those are otherwise not directly accessible in the undoped NP [29, 30]. Of particular interest are the *d*- and *f*-block elements to generate optical materials with interesting emission properties. Presence of suitable dopants among these elements can give rise to additional emission bands compared to that from the NP excitonic and/or surface state emissions. Emissions from d-block elements are generally broad due to efficient mixing with ligand orbitals relaxing the spin selection rule. On the other hand, emissions from f-block elements are unique. These bands are sharp with minimum intra- and inter-Ln^{3+} spectral overlap, span the entire visible and near infrared (NIR) spectral range, longer (microseconds–milliseconds) lifetime allowing time-gated measurements, relatively insensitive to environment, resistant to photobleaching thus allowing longer experiment time and enhancing the signal-to-noise ratio. Lanthanide containing luminophores thus find unique applications in biological imaging, bio-analytical applications, optoelectronics, sensing, lasers, and telecommunications; among others [31–45].

Accessing useful emissions from Ln^{3+} is however challenging due to their inefficient direct excitation [ε (Ln^{3+}) ≤ 10 M^{-1} cm^{-1}, ε (organic fluorophore) ≈ 10^4–10^5 $M^{-1}cm^{-1}$] and environmental vibrational overtone induced emission quenching [34, 46]. One way to address these challenges is to incorporate Ln^{3+} in an appropriate coordination environment, in which by virtue of an efficient excitation of the surrounding entities, energy can be transferred to the Ln^{3+} center. That is, an optical antenna effect can operate to sensitize the Ln^{3+} emission. Various research laboratories are devoting attention to synthesize Ln^{3+} containing inorganic molecules. [47–50] On the other hand, similar beneficial scenario can also be visualized by incorporating (doping) an appropriate Ln^{3+} in a suitable semiconductor NP, in which the NP can act as an optical antenna to sensitize the Ln^{3+} luminescence. These inorganic NPs also act as a protector matrix by offering lower frequency vibrations, and thus environment induced non-radiative processes are largely suppressed [51]. Additionally, these composite host (semiconductor NP) – guest (Ln^{3+}) assemblies benefit from individual properties of the ingredients, and provides avenues of accessing quantum confinement, surface engineering, inclusion of multiple and distinct Ln^{3+} in a given NP. These properties can be explored for targeted therapy and multiplex assays.

During early developments in this field, Bol and co-workers raised an important question on the feasibility of incorporating Ln^{3+} in semiconductor NPs considering the size and charge mismatch of the ingredient cations [52]. Later studies by various research groups demonstrated that an optimization of synthetic protocol can indeed incorporate Ln^{3+} in inorganic NPs [53–60]. In an early seminal demonstration in this research direction, Petoud and co-workers discussed successful Tb^{3+} doping in CdSe NPs [53], in which the NPs are demonstrated to act as the feeding channel to sensitize the Tb^{3+} emission and offer spatial protection from environmental non-radiative deactivation processes. Other such demonstrations include incorporation of Eu^{3+} in TiO_2 [5], Nd^{3+}/Sm^{3+} in TiO_2, [6] Er^{3+} in SnO_2 [61], Eu^{3+} in SnO_2 [62], Er^{3+} in TiO_2 [63], Tb^{3+} in ZnS, [64, 65] Eu^{3+} in ZnS [66–74], Eu^{3+} in CdS [75], Eu^{3+}/Tb^{3+} in CdSe–ZnS [76], Yb^{3+} in surface modified CdSe [77]. The size and charge mismatch can be compensated by lattice distortion and charge compensation. Based on site symmetry consideration, Chen and co-workers discussed how incorporation of Eu^{3+} in TiO_2 NPs can change the Ti^{4+} symmetry of core sites from D_{2d} to either D_2 or C_{2v} and surface sites to C_1 symmetries [5]. Aliovalent doping of Cu^{2+}/Ag^+ in InAs NPs is also characterized by Banin and co-workers [18]. Motivated by the unconventional emission characteristics of Ln^{3+}, we initiated working on developing Ln^{3+} doped semiconductor NPs and understanding the underlying photophysical processes, in order to access materials with predictable and desirable properties. In 2011, Waldeck, Petoud and co-workers reported an analysis to rationalize the photophysical outcome of Tb^{3+} and Eu^{3+} emissions in II-VI sulfide and selenide materials [78].

The experimental observations were rationalized based on a charge trapping mediated sensitization model, in which appropriately positioned Ln^{3+} ground and luminescent energy levels can act as potential hole and electron traps, and the electron-hole pair recombination at these trap sites populates the Ln^{3+} luminescent energy levels thus generating host sensitized dopant emission. This analysis also identifies ZnS being the most efficient host matrix in order to achieve maximum host sensitization. It is further demonstrated that a smaller dimension of NP is beneficial to maximize the sensitized Tb^{3+} emission in ZnS based NPs [79]. We also argued that the spectral overlap of donor NP emission and acceptor Ln^{3+} absorption is insignificant in deciding the spectral outcome of these assemblies [78–81].

These outcomes on synthetically doped Ln^{3+} semiconductor NPs combined with the robustness of post-synthetic modification of inorganic NPs led us to undertake investigations with Ln^{3+} being the incoming cation. These studies are categorized as CA/Ln systems, where Ln after slash indicates their addition post-synthetically to pre-formed NPs. Another obvious scenario arises from treating synthetically Ln doped, C(Ln)A that is Ln mentioned within parenthesis, NPs with M^{n+} to synthesize C(Ln)A/M NPs, and to study how the inclusion of M can tune the photophysical properties of the NP. Different outcomes that can emerge from this reaction formulation include modulation of NP's electronic properties without or with alteration of the NP's core structure. Finally, presence of a surface capping ligand on NPs confers stability and guide NP's dispersion nature. In the photophysical perspective, these capping ligands are known to guide NP's emission extent [82], reaction kinetics [83–85], dopant emission lifetime [86]; and often contains ionisable groups. Such a NP, in the form of 1-thioglycerol (1-TG) capped Zn(Tb)S, is treated post-synthetically to vary the dispersion pH, and its photophysical properties was investigated. Collectively, these experiments yield a comprehensive picture to generate Ln^{3+} semiconductor NP, tune properties of existing Ln^{3+} by either modulating the core or surface of the NPs by using the facile post-synthetic modification strategy. The plan of this perspective with these different facets is summarized in Scheme 1. Population of Ln^{3+} in both core and surface sites of the NPs is evident from the experimental observations (see Discussion below). Both substitutional and interstitial doping is possible for core sites. These aspects are not shown explicitly while constructing the Scheme 1. Future perspectives are also discussed.

Results and discussion

I. CA/Ln NPs: generation of Ln^{3+} doped semiconductor NP luminophores

(i) ZnS/Ln [Ln = Tb, Eu]. The knowledge of ZnS NPs' ability to sensitize synthetically doped Tb^{3+} and Eu^{3+} [78] led a platform to treat ZnS NPs post-synthetically with Tb^{3+}/Eu^{3+}. In 2013, Waldeck, Petoud and co-workers reported the observations from experiments in which the ZnS NPs were treated post-synthetically by adding Tb^{3+}/Eu^{3+} nitrates, with their quantities matching the corresponding synthetically doped cases [87]. Most interestingly, noticeable Tb^{3+} and Eu^{3+} emissions are observed from the ZnS/Tb and ZnS/Eu NPs. The emission spectra of the ZnS, ZnS/Tb, and ZnS/Eu NPs are shown in panel (b) of Figure 1. Clearly, in the ZnS/Tb NPs sharp Tb^{3+} emission bands are visible that are centered at 490, 545, 585, and 620 nm that originates from the $^5D_4 \rightarrow {}^7F_n$ [$n = 6$–3] transitions, in addition to the broad blue emission of ZnS emissive center. Similarly, the sharp Eu^{3+} emissions appear at 590, 616, and 700 nm that originates from the $^5D_0 \rightarrow {}^7F_n$ [$n = 1, 2, 4$] transitions. The excitation spectra, while monitoring the Ln^{3+} emission bands are shown in panel (a) of Figure 1. Corresponding spectra for the undoped ZnS NPs are also included. These spectra primarily reveal a broad profile that overlap significantly with that of the NPs, without significant contributions from direct sharp 4f–4f bands. This unequivocally suggests that the ZnS NPs act as a feeding channel to sensitize either Tb^{3+} or Eu^{3+} emissions. That is, an optical antenna effect operates in these assemblies. The post-synthetically modified ZnS/Tb NPs (taken as a representative system) are stable over time. Acquisition of emission spectra even after ~2.5 months of post-synthetic modification shows no degradation of the Tb^{3+} emission. Panel (c) of Figure 1 shows the trend in Eu^{3+} emission when gradually ZnS NPs are added to the solution of Eu^{3+} nitrates in chloroform. An increase in Eu^{3+} emission is observed that is correlating with the amount of NPs present in the chloroform dispersion.

In order to evaluate the extent of spatial protection that these NPs can offer to the Ln^{3+}, the Ln^{3+} emission lifetimes in the ZnS/Tb and ZnS/Eu NPs are acquired, and the corresponding decay profiles are compared to that obtained for the freely floating Tb^{3+}/Eu^{3+} in bulk solvent, which are shown in panel (d) of Figure 1. The lifetimes for Tb^{3+} and Eu^{3+} emissions in bulk solvent are found to be 250 and 125 μs, respectively. In presence of ZnS NPs, these lifetimes are significantly lengthened, and they are found to be bi-exponential in nature. Specifically, Tb^{3+} and Eu^{3+} emission lifetime components are found to be 500 μs and 2.4 ms, and 500 μs and 1.5 ms, for the ZnS/Tb and ZnS/Eu NPs, respectively. These two lifetime components can arise from different spatial location of Ln^{3+} in the NPs. That is, while the surface localized Ln^{3+} are more prone to environment induced non-radiative deactivation pathways generate a shorter lived emission, the core localized Ln^{3+} can produce much longer lifetime due to better spatial protection. In well protected molecular complexes, Tb^{3+} and Eu^{3+} emission lifetimes were found to be 1.3 and 0.78 ms, respectively [88]. This clearly indicates that the Tb^{3+}/Eu^{3+} emissions are well protected in the ZnS NPs even when the Ln^{3+} precursors are added post-synthetically to the pre-formed NPs.

(ii) CdS/Ln [Ln = Tb, Eu]. Generality of these observations and usefulness of this post-synthetic modification strategy to generate Ln^{3+} doped inorganic NP luminophores is examined by undertaking experiments in which the CdS NPs are post-synthetically treated with Tb^{3+}/Eu^{3+} separately. The emission spectra from these

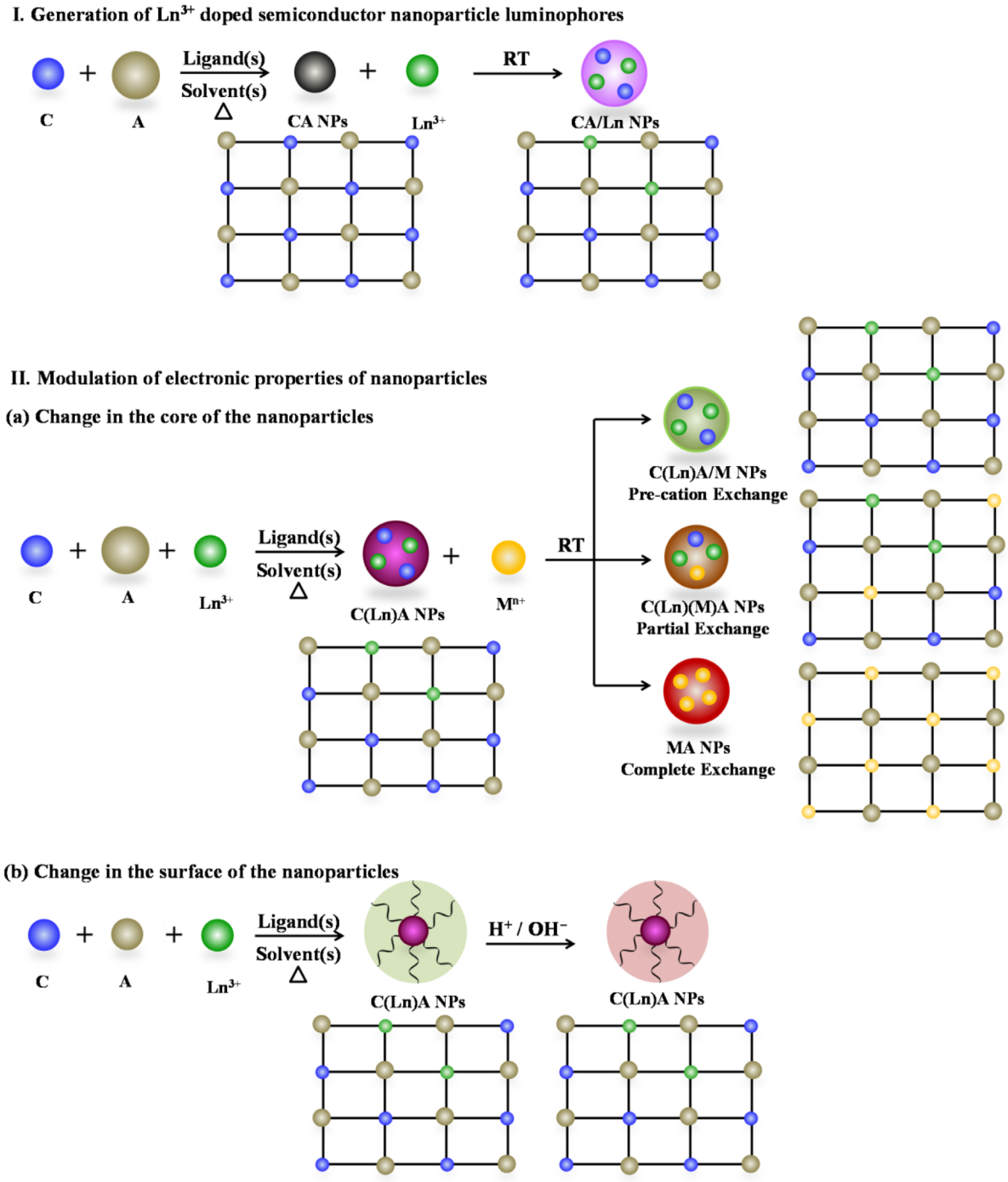

Scheme 1. Different post-synthetic reaction strategies (*RT* stands for room temperature).

measurements are shown in panel (f) of Figure 1. Remarkable enhancement of Tb^{3+}/Eu^{3+} emissions are observed in presence of the NPs, compared to that observed in the freely floating Tb^{3+}/Eu^{3+}. The excitation spectra, while monitoring the Tb^{3+}/Eu^{3+} emissions are shown in panel (e) of Figure 1. Corresponding electronic absorption spectrum is also included. Similar to the ZnS NPs case, these profiles are also broad without noticeable contributions from direct sharp 4f–4f excitation bands. Most remarkably, these spectra identify bands at the lowest energy excitonic band maxima of the CdS NPs centered at 360 nm. Thus, these spectra affirmatively confirm operation of an optical antenna effect to sensitize Tb^{3+}/Eu^{3+} emissions by the CdS NPs.

(iii) Role of Spatial Position: A Case Study with Eu^{3+} Doped NPs. It is important to evaluate the role of Ln^{3+} spatial position in deciding the photophysical outcome in the CA/Ln NPs. Correspondingly a comparative analysis

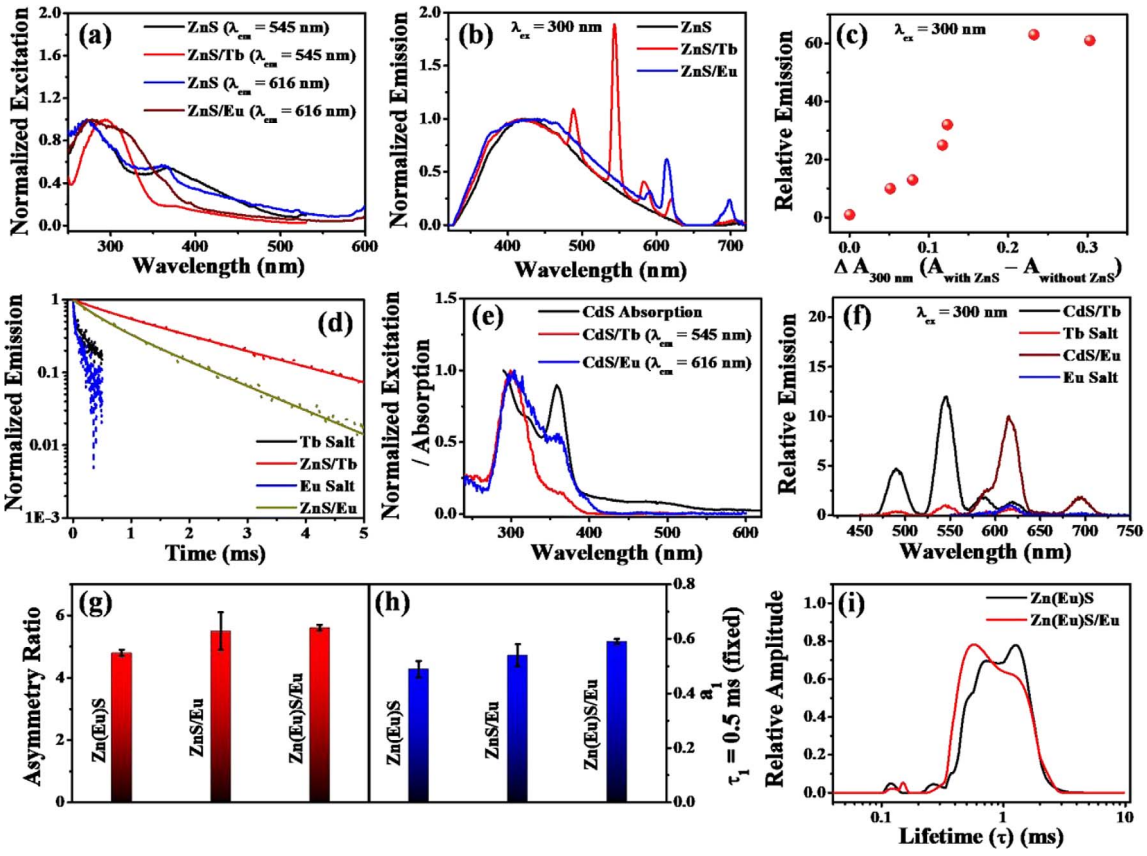

Figure 1. Luminescence excitation and emission spectra of the ZnS, ZnS/Tb, and ZnS/Eu NPs are shown in panels (a) and (b), respectively. Panel (c) shows the Eu^{3+} emission trend when ZnS NPs are gradually added to the dispersion. The Ln^{3+} emission lifetime decay profiles in the ZnS/Tb and ZnS/Eu NPs are shown in panel (d), with the corresponding profiles of freely floating Ln^{3+} included. Luminescence excitation and emission spectra of the post-synthetically treated CdS/Tb and CdS/Eu NPs are shown in panels (e) and (f), respectively. The electronic absorption spectrum of the CdS NPs is also included in panel (e) for comparison. Panels (g), (h), and (i) show the trends in Eu^{3+} asymmetry ratio, emission lifetime, and emission lifetime distribution, respectively. (Adapted with permission from Reference [87], Copyright 2013 American Chemical Society).

is undertaken between the ZnS/Eu and Zn(Eu)S NPs: in the form of asymmetry ratio (ratio of integrated emission intensity of the Eu^{3+} electric and magnetic dipole transitions centered at 616 and 590 nm, respectively) [34, 89], emission lifetime, and lifetime distribution analysis. A summary of these analyses are presented in the panels (g)–(i) of Figure 1. The intensity of electric dipole transition increases in an asymmetric environment, while the intensity of the magnetic dipole transition remains unaffected. Correspondingly, an increase in asymmetry ratio can be correlated with an asymmetric co-ordination environment around Eu^{3+}. The Eu^{3+} asymmetry ratio values are found to be 4.8 ± 0.1, 5.5 ± 0.6, and 5.6 ± 0.1 in the Zn(Eu)S, ZnS/Eu, and Zn(Eu)S/Eu NPs, respectively. Thus, a more asymmetric environment is experienced by Eu^{3+} when they are added post-synthetically, compared to the synthetically doped NPs. In corroboration to the trends in asymmetry ratio values, the contribution of shorter surface related lifetime component increases in the post-synthetically added NPs, compared to that in the synthetically doped Zn(Eu)S NPs. A more realistic scenario is to visualize Ln^{3+} being randomly distributed in the NPs, rather discretely localized at specific core and surface sites of the NPs. Lifetime distributions are hence compared. Clearly, contributions of shorter lifetime components are increased in the Zn(Eu)S/Eu compared to that in the Zn(Eu)S NPs. These data cumulatively indicate a small yet discernible enhanced surface population of Eu^{3+} in the post-synthetically treated NP, compared to that in the synthetically doped counterparts.

(iv) CdSe/Ln and ZnS/Ln [Ln = Pr, Nd, Sm, Eu, Tb, Dy, Ho, Er, Tm, Yb]. While the experiments described above clearly demonstrate the usefulness of post-synthetic reaction strategy to develop Ln^{3+} containing semiconductor NPs, these data do not identify the (a) extent of Ln incorporation in the NPs and more specifically the fate of NP's elemental composition due to the introduction of Ln, (b) feasibility of realizing host sensitized emissions in other Ln^{3+} besides Tb^{3+} and Eu^{3+}, and (c) hence unravelling the underlying photophysical processes. In order to address these questions more comprehensively, we performed experiments in which the CdSe and ZnS NPs were treated post-synthetically by adding an excess (100 and 5 times for the CdSe and ZnS NPs, respectively) amount of

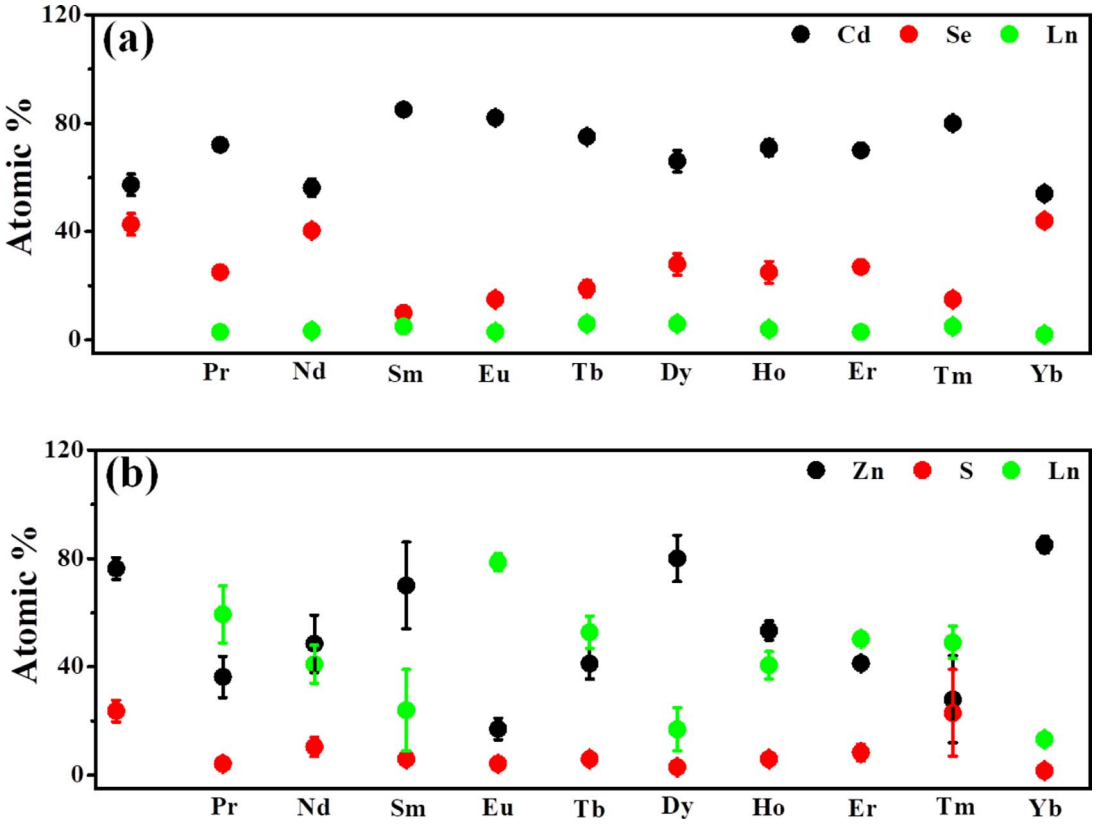

Figure 2. Elemental composition of the CdSe/Ln and ZnS/Ln, as determined from the EDS measurements are shown in panels (a) and (b), respectively. (Adapted with permission from Reference [90], Copyright 2019 Elsevier).

Ln^{3+} [Ln = Pr, Nd, Sm, Eu, Tb, Dy, Ho, Er, Tm, Yb] nitrates [90]. Post-synthetic modification of the CdSe NPs with diameter of 2.2 ± 0.3 nm by Tb^{3+} resulted in the CdSe/Tb NPs with a diameter of 2.6 ± 0.4 nm. Similarly, corresponding values for the ZnS and ZnS/Tb NPs were found to be 2.2 ± 0.4 and 2.5 ± 0.4 nm, respectively. We note that the NPs dimension are almost very similar following the post-synthetic addition of Ln^{3+} to either the CdSe or ZnS NPs, and the change in NP's diameter of ~15% does not have significant impact on their colloidal stability.

(a) Elemental Composition. The elemental composition of the CdSe/Ln and ZnS/Ln NPs, as obtained from the energy dispersive X-ray spectroscopy (EDS), are shown in panels (a) and (b) of Figure 2, respectively. All the CdSe/Ln and ZnS/Ln NPs capture incorporation of Ln in the NPs. However, a difference in extent of Ln introduction is noticed as a function of host. While CdSe incorporates them in smaller amounts, their values are higher in the ZnS NPs. Complete cation exchange of either Cd^{2+}/Zn^{2+} by Ln^{3+} is not evident. Moreover, significant alteration in the anionic framework is noticed upon addition of Ln^{3+} to these NPs.

A simple estimation of predicting the feasibility of Cd^{2+}/Zn^{2+}–Ln^{3+} exchange on thermodynamic considerations [21] gives rise to a reaction free energy value that is close to zero [90], suggesting that this cation exchange is not a favorable process. Thus, observation of absence of complete exchange of Cd^{2+}/Zn^{2+} by Ln^{3+} is justifiable. A remarkable alteration of the anionic framework of the NPs in both the cases are noteworthy, with formation of cation rich NPs. The diffusion co-efficient of Cd^{2+}, Zn^{2+}, and Ln^{3+} are 0.72 × 10^{-5} cm^2 s^{-1}, 0.70 × 10^{-5} cm^2 s^{-1}, and (0.58–0.62) × 10^{-5} cm^2 s^{-1}, respectively. This suggests that the inward cation diffusion of Ln^{3+} is slower compared to that of the outward diffusion of Cd^{2+}/Zn^{2+} from the NPs. That is, a nanoscale Kirkendall effect operates [23, 91, 92]. The diffusion co-efficient of S^{2-} is 0.73 × 10^{-5} cm^2 s^{-1}. In this post-synthetic modification process of the NPs, Zn^{2+} extracts S^{2-}. This most likely associates with greater affinity of Zn^{2+} to S^{2-}, compared to that of Ln^{3+}. This reorganization of NPs is probably kinetically favored.

(b) Luminescence. The steady-state emission spectra of the CdSe and CdSe/Ln [Ln = Pr, Nd, Sm, Eu, Tb, Dy, Ho, Er, Tm, Yb] NPs are shown in panels (c) and (d) of Figure 3. CdSe NPs show an excitonic band maximum at 510 nm. Addition of Ln^{3+} diminishes this band to a significant extent, and only a small contribution is noticed. This is consistent with partial cation exchange of Cd^{2+} by Ln^{3+} in generating the CdSe/Ln NPs. Introduction of Ln^{3+} in the NPs generally alters the emission characteristics, with a blue shifted much broader emission contribution. Among all the CdSe/Ln NPs investigated, only Tb^{3+} and Eu^{3+} show sensitized emission. This can be tracked by monitoring the excitation spectra, as shown in panel (a) of Figure 3. While monitoring the respective emission bands these spectra yield a broad spectrum without contributions from

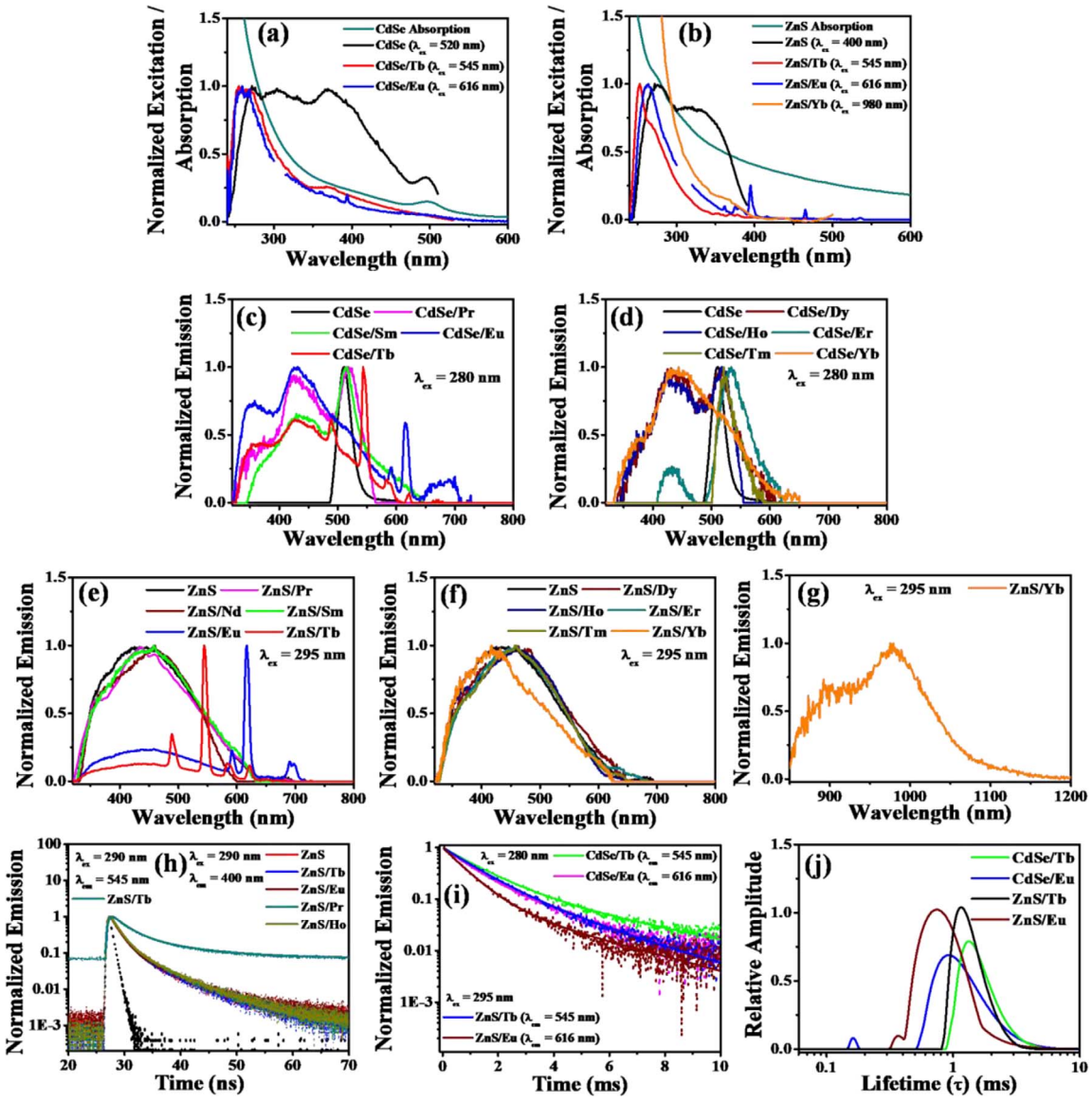

Figure 3. The luminescence excitation and emission spectra of the CdSe/Ln and ZnS/Ln [Ln = Pr, Nd, Sm, Eu, Tb, Dy, Ho, Er, Tm, Yb] NPs are shown in panels (a)–(g), respectively. The electronic absorption spectra of the CdSe and ZnS NPs are also included in panels (a) and (b) for comparison. The shorter time decay kinetics of the ZnS and ZnS/Ln [Ln = Tb, Eu, Pr, Ho] to monitor the NP's intrinsic depopulation rates are shown in panel (h). Panel (i) shows the longer time decay profiles of the CdSe/Ln and ZnS/Ln [Ln = Tb, Eu] NPs to monitor the Tb^{3+} and Eu^{3+} depopulation rates. Panel (j) shows the lifetime distribution analysis of the Tb^{3+} and Eu^{3+} emissions. (Adapted with permission from Reference [90], Copyright 2019 Elsevier).

sharp direct 4f–4f bands, suggesting operation of an optical antenna effect. Furthermore, similar to the CdS/Ln [Ln = Tb, Eu] NPs discussed above, these excitation spectra capture signature of first excitonic absorption band, strengthening the argument of NPs induced sensitization effect.

The corresponding emission spectra in the ZnS/Ln [Ln = Pr, Nd, Sm, Eu, Tb, Dy, Ho, Er, Tm, Yb] NPs are shown in panels (e) and (f) of Figure 3. ZnS NP's emit at blue spectral range with a maximum around 420 nm. This broad blue emission is correlated primarily with sulfur vacancies, however contributions from zinc and sulfur interstitials and zinc vacancies is also discussed [27, 93–95]. Higher and lower energy contributions originate from the roles of interstitial and vacancy sites, respectively. Introduction of Ln in the ZnS/Ln NPs do not alter this surface state composition to a significant extent. Among the ZnS/Ln NPs, Tb^{3+}, Eu^{3+}, and Yb^{3+} show sensitized emission. The Yb^{3+} emission from the ZnS/Yb NPs is shown in panel (g) of Figure 3. The sensitization effect is confirmed by acquiring the respective excitation spectra while monitoring the Ln^{3+} emission bands. These spectra are shown in panel (b) of Figure 3. While generating the CdSe/Ln and ZnS/Ln NPs, the CdSe or ZnS NPs were post-synthetically treated with an excess amount of incoming Ln^{3+} cations, to drive the reaction as much as possible to the product side. Thus these reactions do not directly probe the doping extent

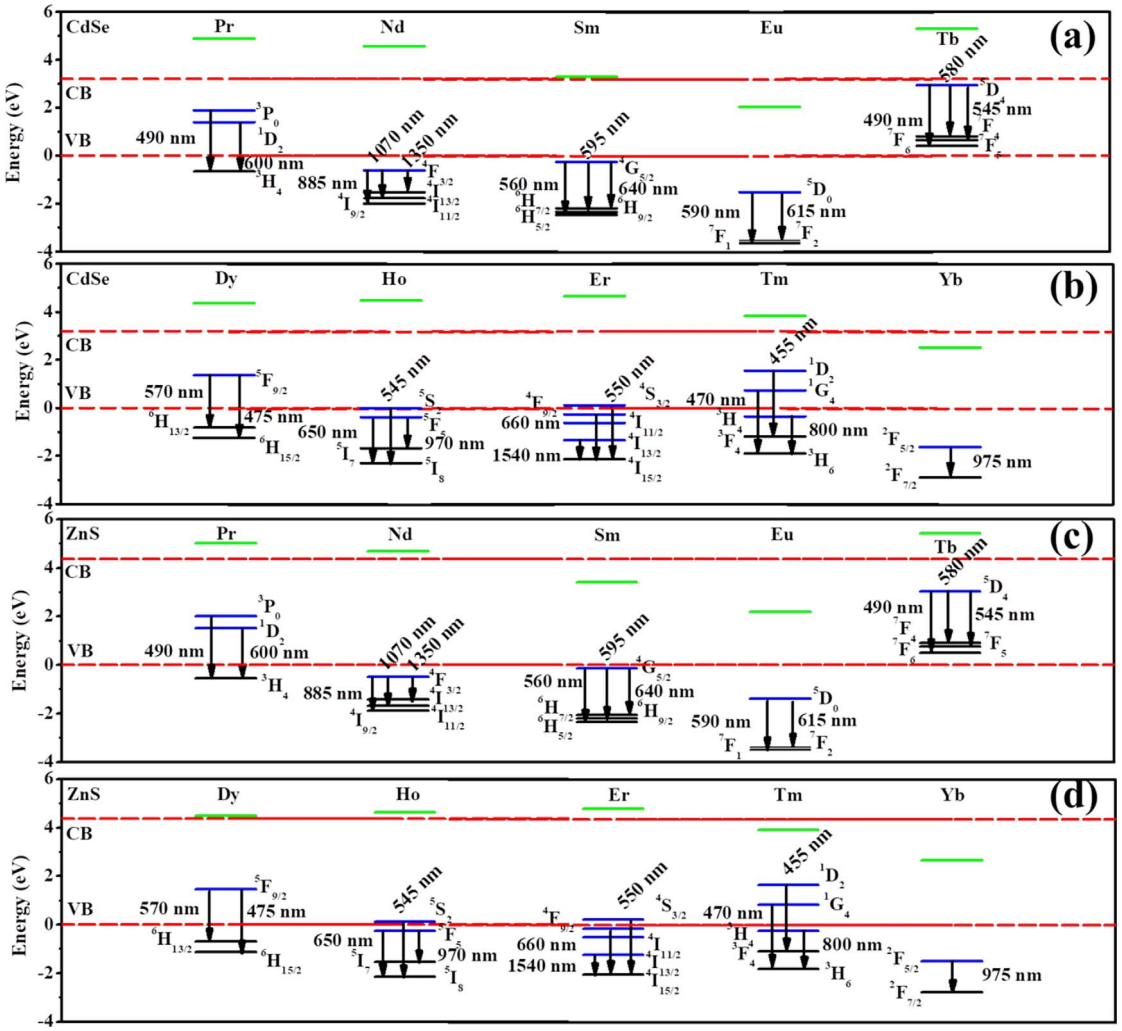

Figure 4. Relative energy level schematic with placement of Ln^{3+} ground and luminescent energy levels with respect to the valence and conduction bands of the host material is shown. Ground and luminescent energy levels in each case are represented by black and blue solid lines, respectively. Prominent luminescence transitions are shown with downward arrows in each case. Ln^{2+} ground energy levels are indicated by green horizontal lines. These energy levels are positioned following a method proposed by Dorenbos [96, 97] and later adopted by us, [78–81, 90, 98] and relies on inputs of host independent universal binding energy trend of Ln^{3+} and the charge transfer energy from anion valence band of host material to Ln^{3+} moieties. (Adapted with permission from Reference [90], Copyright 2019 Elsevier).

dependence on the optical properties of these NPs. A systematic investigation to decipher this aspect would be extremely interesting and we consider this as a future direction.

The shorter time dynamics of the ZnS and ZnS/Ln [Ln = Tb, Eu, Pr, Ho] NPs are measured by exciting the NPs at 290 nm and collecting the broad ZnS centered emissions at 400 nm. These decay profiles are shown in panel (h) of Figure 3. All these decay profiles are similar, with an average emission lifetime in the range of tenths of picoseconds. This suggest that operation of sensitization in Tb^{3+}/Eu^{3+} cases do not impact ZnS decay kinetics. Collecting the emission at 545 nm, a wavelength where Tb^{3+} emits, only shifts the baseline and produces lifetimes in the range of picoseconds. The Ln^{3+} emission lifetimes in the CdSe/Ln and ZnS/Ln [Ln = Tb, Eu] are measured with a set-up having lower repetition rate of the excitation source to monitor the longer time decay dynamics. These decay profiles are shown in panel (i) of Figure 3. All these decay profiles reveal bi-exponential decay kinetics, where the shorter and longer lifetime decay components are correlated with the lesser and more protected surface and core sites of the NPs, respectively. The lifetime distribution analysis from these decays is shown in panel (j) of Figure 3. The lifetime decays and their distribution analyses suggest that CdSe NPs offer better spatial protection to the Tb^{3+} / Eu^{3+} emissions. The radiative rates of NP are approximately million times faster than that of the Ln^{3+} emissive centers, thus they remain unaffected even in presence of Ln^{3+} sensitized emissions from the doped NPs.

(c) Photophysical Rationalization. In the context of realizing host sensitized Ln^{3+} emissions, it is remarkable to note

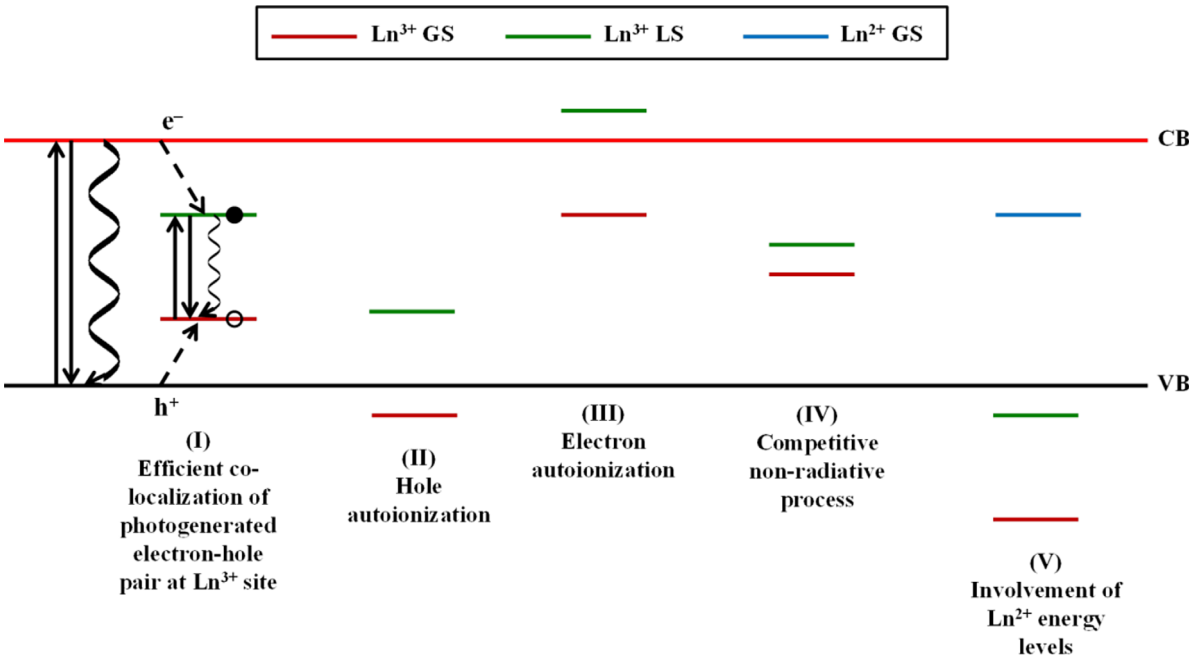

Scheme 2. Plausible charge trapping scenarios in doped semiconductor NPs.

that this is only observed in the CdSe/Tb, CdSe/Eu, ZnS/Tb, ZnS/Eu, and ZnS/Yb NPs. Other NPs among the CdSe/Ln and ZnS/Ln [Ln = Pr, Nd, Sm, Dy, Ho, Er, Tm] do not show host sensitized Ln^{3+} emissions. These observations are rationalized within a charge trapping mediated dopant emission sensitization mechanism. The Ln^{3+} energy levels are placed with respect to the NP's valence and conduction bands following a method proposed by Dorenbos and co-workers [96, 97] and later adopted by us. [78–81, 90, 98]

The key assumptions in this semi-empirical approach are as follows. (i) The binding energy trend of Ln^{3+} is universal and is host independent. This is by virtue of the core like feature of the 4f electrons. (ii) The charge transfer energy from the anion valence band to Eu^{3+} is equal to the energy difference between the valence band of the host material and the Eu^{2+} ground energy level in that material, and (c) the energy difference between the Eu^{2+} and Eu^{3+} ground energy levels in lower band gap materials is equal to 5.7 eV. With these inputs and known band gap value of a host material, all the Ln^{3+} and Ln^{2+} ground energy levels can be placed with respect to the valence and conduction bands of the host material. The higher lying Ln^{3+} energy levels can be placed accordingly following the reports by Rajnak and co-workers [99–101]. Such energy level schematics are constructed for the CdSe/Ln and ZnS/Ln [Ln = Pr, Nd, Sm, Eu, Tb, Dy, Ho, Er, Tm, Yb] NPs, and are shown in Figure 4.

Important energy offsets in this model are the energy differences between the top of the valence band and the Ln^{3+} ground energy level (ΔE_1) and between the bottom of the conduction band and the Ln^{3+} luminescent energy level (ΔE_2). An optimum negative and positive value of ΔE_1 and ΔE_2 ensure effective co-localization of photogenerated hole and electron at the Ln^{3+} ground and luminescent energy levels, respectively. Subsequent electron-hole pair recombination at the Ln^{3+} related trap site populates the Ln^{3+} luminescent energy level, thus producing host sensitized dopant emission from the doped NPs. It is important for these energy offsets to be optimum, as a lower and higher value would result in back charge transfer and experience detrimental effects from competitive non-radiative relaxation processes. Another scenario may arise when these energy levels are buried in one of the bands. For example, if the luminescent energy level of a particular Ln^{3+} lies above the conduction band of the host material, then the photogenerated electron would experience auto-ionization effect, thus reducing the Ln^{3+} emission efficiency. These different scenarios are summarized in Scheme 2.

A close inspection of the energy level schematic in Figure 4 reveals a favourable energy level alignment in Tb^{3+}, where the ground and luminescent energy levels $^7F_6$ and $^5D_4$ are positioned suitably above and below the valence and conduction bands of both CdSe and ZnS NP host. In cases of Nd^{3+}, Sm^{3+}, Eu^{3+}, Dy^{3+}, Ho^{3+}, Er^{3+}, Tm^{3+}, Yb^{3+} the ground energy level is buried in the valence band, thus they are prone to experiencing auto-ionization of the photogenerated hole. In case of Pr^{3+} ΔE_1 is marginally negative, thus also contributing detrimentally. Thus, only Tb^{3+} ground energy level can act as a potential hole trap in either CdSe/ZnS NP host. The values of ΔE_2 is very large in cases of Nd^{3+}, Sm^{3+}, Eu^{3+}, Dy^{3+}, Ho^{3+}, Er^{3+}, Yb^{3+}, implying roles of competitive relaxation pathways through NP's various surface states. This ΔE_2 value is not severely adverse in cases of Pr^{3+} and Tm^{3+}. An additional energy level of importance comes in picture for

Table 1. Summary of relevance of ΔE_1, ΔE_2, and ΔE_3 in CdSe and ZnS NPs.

Host	Dopant (Ln^{3+})	ΔE_1 [E (VB)–E (Ln^{3+} Ground Energy Level) [Hole trapping]	ΔE_2 [E (CB)–E (Ln^{3+} Luminescent Energy Level) [Electron trapping]	ΔE_3 [E (CB)–E (Ln^{2+} Ground Energy Level) [Alternate excitation pathway through involvement of Ln^{2+} ground energy level]
CdSe/ZnS	Pr^{3+}	Marginally not suitable	Marginally suitable	Not suitable
CdSe/ZnS	Nd^{3+}	Not suitable	Not suitable	Not suitable
CdSe/ZnS	Sm^{3+}	Not suitable	Not suitable	Suitable
CdSe/ZnS	Eu^{3+}	Not suitable	Not suitable	Suitable
CdSe/ZnS	Tb^{3+}	Suitable	Suitable	Not suitable
CdSe/ZnS	Dy^{3+}	Not suitable	Not suitable	Not suitable
CdSe/ZnS	Ho^{3+}	Not suitable	Not suitable	Not suitable
CdSe/ZnS	Er^{3+}	Not suitable	Not suitable	Not suitable
CdSe/ZnS	Tm^{3+}	Not suitable	Marginally suitable	Marginally suitable
CdSe/ZnS	Yb^{3+}	Not suitable	Not suitable	Suitable, better in ZnS [5240 cm^{-1} in CdSe/Yb and 13,710 cm^{-1} in ZnS/Yb]

Sm^{3+}, Eu^{3+}, Tm^{3+}, Yb^{3+} where the respective Ln^{2+} ground energy levels lie within the band gap. The relevant energy difference, ΔE_3, is between the conduction band of the host NP and the Ln^{2+} ground energy level. An optimum positive value of ΔE_3 offers an additional excitation pathway to populate the Ln^{3+} luminescent energy levels by the involvement of Ln^{2+} ground energy levels. The relevance of ΔE_1, ΔE_2, and ΔE_3 in CdSe and ZnS NPs are summarized in Table 1.

Besides the efficiency of trapping photogenerated charge carriers at Ln^{3+} related energy levels, another important consideration comes from the environment induced emission quenching of Ln^{3+}. In this regard, the energy difference between the luminescent energy level and the highest spin orbit level of the ground energy level is of importance. This energy difference is represented as ΔE_4, and the ΔE_4 values for different Ln are tabulated in Table 2. A lower value of ΔE_4 correlates to higher quenching efficiency.

Based on the photophysical outcome, the following steps are proposed for the Ln^{3+} emission sensitization in semiconductor NPs, where the Ln^{3+} ground and luminescent energy levels are optimally placed above and below the valence and conduction band of the host NPs.

(1) Excitation of semiconductor NP and generation of electron-hole pair

$$\mathrm{Zn(Ln)S} + h\nu \rightarrow \mathrm{ZnS}\ [h^+ + e^-]$$

(2) Hole trapping at the dopant site followed by electron trapping from a non-dopant site and creation of the excited Ln^{3+}

$$Ln^{3+} + h^+ \rightarrow [Ln^{3+} + h^+ \Leftrightarrow Ln^{4+}]$$

$$[Ln^{3+} + h^+ \Leftrightarrow Ln^{4+}] + e^- \rightarrow Ln^{3+*}$$

(3) Electron trapping at the dopant site followed by hole trapping from a non-dopant site and creation of the excited Ln^{3+}

$$Ln^{3+} + e^- \rightarrow \left[Ln^{3+} + e^- \Leftrightarrow Ln^{2+}\right]$$

$$\left[Ln^{3+} + e^- \Leftrightarrow Ln^{2+}\right] + h^+ \rightarrow Ln^{3+*}$$

(4) Electron-hole pair recombination at the dopant site and creation of the excited Ln^{3+}

$$Ln^{3+} + [h^+ + e^-] \rightarrow Ln^{3+*}$$

(5) Luminescence from the Ln^{3+} excited energy level

$$Ln^{3+*} \rightarrow Ln^{3+} + h\nu$$

It is proposed that the sensitization is most effective with process (4) is in operation. Such is the case in the Zn(Tb)S NPs. In short, the experiments with ZnS/Ln [Ln = Pr, Nd, Sm, Eu, Tb, Dy, Ho, Er, Tm, Yb], CdS/Ln [Ln = Eu, Tb], and CdSe/Ln [Ln = Pr, Nd, Sm, Eu, Tb, Dy, Ho, Er, Tm, Yb] NPs reveal generation of Ln semiconductor NP based luminophores with (a) facile incorporation of Ln in the NPs and (b) realization of host sensitized Ln^{3+} emission in ZnS/Ln [Ln = Eu, Tb, Yb], CdS/Ln [Ln = Eu, Tb], and CdSe/Ln [Ln = Eu, Tb] NPs that can be rationalized by a charge trapping mediated dopant emission sensitization mechanism.

II. Modulation of the Electronic Properties of NPs

A. Zn(Tb)S/M NPs : Core Alteration. Modifying an inorganic NP post-synthetically can access nanomaterials of unique properties. A favorable combination of existing and added cation pair can result in cation exchange [7], feasibility of which can be predicted based on thermodynamic consideration [21, 23]. Dimensional advantage additionally ensures a kinetically facile reaction. That is, these reactions oftentimes happen at or near ambient conditions. On the other hand, even when such an exchange is not happening, post-synthetic modification of the NPs can simply tune the surface state composition of the NPs. Considering a large surface-to-volume ratio surface atoms are of significant contribution in dictating the overall properties of the NPs. Thus, understanding the implications of post-synthetic modification process on the luminescence behavior of the NPs is of interest. We first performed experiments in which the 1-thioglycerol (1-TG) capped Zn(Tb)S NPs are post-synthetically modified by Pb^{2+}, Hg^{2+}, Cd^{2+}, Ca^{2+}, Mg^{2+},

Table 2. Energy difference considerations for different Ln related to environment induced emission quenching.

	ΔE_4 (cm^{-1})									
	Ln [initial energy level (i), final energy level (f)]									
Pr	Nd	Sm	Eu	Gd	Tb	Dy	Ho	Er	Tm	Yb
6940 [$^1D_2$, $^1G_4$]	5410 [$^4F_{3/2}$, $^4I_{15/2}$]	[$^4G_{5/2}$, $^6F_{11/2}$]	12300 [$^5D_0$, $^7F_6$]	32200 [$^6P_{7/2}$, $^8S_{7/2}$]	15100 [$^5D_4$, $^7F_0$]	7850 [$^4F_{9/2}$, $^6F_{3/2}$]	3000 [$^5S_2$, $^5F_5$]	3100 [$^4S_{3/2}$, $^4F_{9/2}$]	6650 [$^1D_2$, $^1G_4$]	10240 [$^2F_{5/2}$, $^2F_{7/2}$]
3910 [$^3P_0$, $^1D_2$]							2200 [$^5F_5$, $^5I_4$]	2850 [$^4F_{9/2}$, $^4I_{9/2}$]	6250 [$^1G_4$, $^3F_2$]	
								6490 [$^4I_{13/2}$, $^4I_{15/2}$]	4300 [$^3H_4$, $^3H_5$]	

Na^+, and K^+ individually [102]. These experiments suggest that the cation exchange of Zn^{2+} by $Pb^{2+}/Hg^{2+}/Cd^{2+}$ is feasible. Two test cases, Zn(Tb)S/Pb and Zn(Tb)S/Cd, are considered that involves changing the NP's interior due to cation exchange. Cation exchange reactions are typically performed with comparable or excess amount of incoming cations. We approached studying these reactions in two relative reactant concentration regimes. First one is the pre-cation exchange regime with sub-stoichiometric reactant concentration range and second one is the cation exchanged counterparts where the NPs are treated with equimolar or excess amount of incoming cations.

(1) Zn(Tb)S/Pb NPs. In 2018, we reported experimental observation from the Zn(Tb)S NPs that is post-synthetically treated with Pb^{2+} to form Zn(Tb)S/Pb NPs [102]. The [Zn(Tb)S]:[Pb^{2+}] was varied from $1:10^{-5}$–1:10. The elemental composition of these NPs based on EDS measurements is shown in panel (a) of Figure 5. In the range of [Zn(Tb)S]:[Pb^{2+}] = $1:10^{-5}$–$1:10^{-2}$, Zn and Tb amounts show near constancy. When this ratio reaches $1:10^{-1}$, Zn starts getting exchanged by Pb, and the NPs with 1:1 and 1:10 reactant concentration ratio essentially tracks completely cation exchanged NPs. That is, the NPs with [Zn(Tb)S]:[Pb^{2+}] = $1:10^{-5}$–$1:10^{-2}$, $1:10^{-1}$–1:1, and >1:1 monitors NPs with no cation exchange, partially cation exchanged, and completely cation exchanged NPs. The XRD profiles of the Zn(Tb)S and the NPs with [Zn(Tb)S]:[Pb^{2+}] = 1:1 are shown in panel (b) of Figure 5. While the Zn(Tb)S NPs exhibit diffraction pattern that is characteristic of a cubic ZnS phase, the Pb containing NPs develop distinct PbS phases with disappearance of ZnS phases. This further corroborates with the cation exchange process. Gradual addition of Pb^{2+} to the Zn(Tb)S NPs with diameter of 3.0 ± 0.5 nm with [Zn(Tb)S]:[Pb^{2+}] = $1:10^{-4}$, $1:10^{-2}$ resulted in the Zn(Tb)S/Pb NPs with diameters of 3.0 ± 0.5 nm, 3.2 ± 0.4 nm, respectively. Further addition of Pb^{2+} with corresponding reactant concentration ratio of 1:1 yields Pb(Tb)S NPs with diameter of 3.9 ± 0.6 nm. These indicate that formation of PbS phase following cation exchange from the Zn(Tb)S NPs increases the particle dimension marginally, most likely reflecting the increase in lattice parameter (5.406 Å and 5.936 Å for cubic ZnS and PbS, respectively).

The luminescence excitation and emission spectra of the Zn(Tb)S and Zn(Tb)S/Pb NPs are shown in panels (c)–(e) of Figure 5. Zn(Tb)S NPs exhibit characteristic broad blue emission from ZnS center and sharp emissions from Tb^{3+} center. All the post-synthetically modified NPs in the pre-cation exchange range show similar spectral pattern, albeit with varying emission efficiency. The excitation spectra, while monitoring the Tb^{3+} emission at 545 nm, reveal a broad profile that has overlap with that obtained by monitoring the ZnS emission at 400 nm. This suggests presence of a host sensitization. In the cation exchanged NPs, the emission from both the ZnS and Tb^{3+} centers are greatly diminished. The emission quantum yield values of ZnS and Tb^{3+} centers are shown in panels (f) and (g) of Figure 5, respectively. It is remarkable to note that even in presence of a small amount of Pb in the NPs, a rich photophysics evolves. For example, the ZnS broad emission decreases with respect to that in the Zn(Tb)S NPs even in the NPs with [Zn(Tb)S]:[Pb^{2+}] = $1:10^{-4}$–$1:10^{-2}$. On the other hand, most interestingly, Tb^{3+} emission is additionally sensitized in presence of Pb. This effect is more pronounced in the NPs with [Zn(Tb)S]:[Pb^{2+}] = $1:10^{-3}$–$1:10^{-2}$. Efforts on detailed understanding of this Pb induced Tb^{3+} emission brightening in ZnS NPs is currently underway in our laboratory. Further increase in [Pb^{2+}] adversely affects the Tb^{3+} emission. Two factors contribute to this. First, a reduced Tb content once [Zn(Tb)S]:[Pb^{2+}] reaches ~1:1, and second being the unfavourable energy level alignment (*vide infra*).

A fascinating direction with cation exchange in inorganic NPs is the ability of reverse cation exchange. Alivisatos and co-workers reported transformation of CdSe → Ag_2Se → CdSe NPs by treating the Ag_2Se with an excess of Cd^{2+} [7]. Although this reaction recovers the CdSe NPs, yet their photophysical properties differ to that of the initial CdSe NPs significantly. For example, the initial NPs only exhibit excitonic emission; however the recovered NPs show an additional contribution from a red shifted emission band. Our efforts to treat the NPs with [Zn(Tb)S]:[Pb^{2+}] = 1:1 with an excess of Zn^{2+} and Tb^{3+}, as shown in panel (h) of Figure 5, indeed recovers emission properties of Zn(Tb)S. However, key differences between the photophysical properties of these NPs with that of the recovered NPs are evident. These include a red shifted ZnS emission and

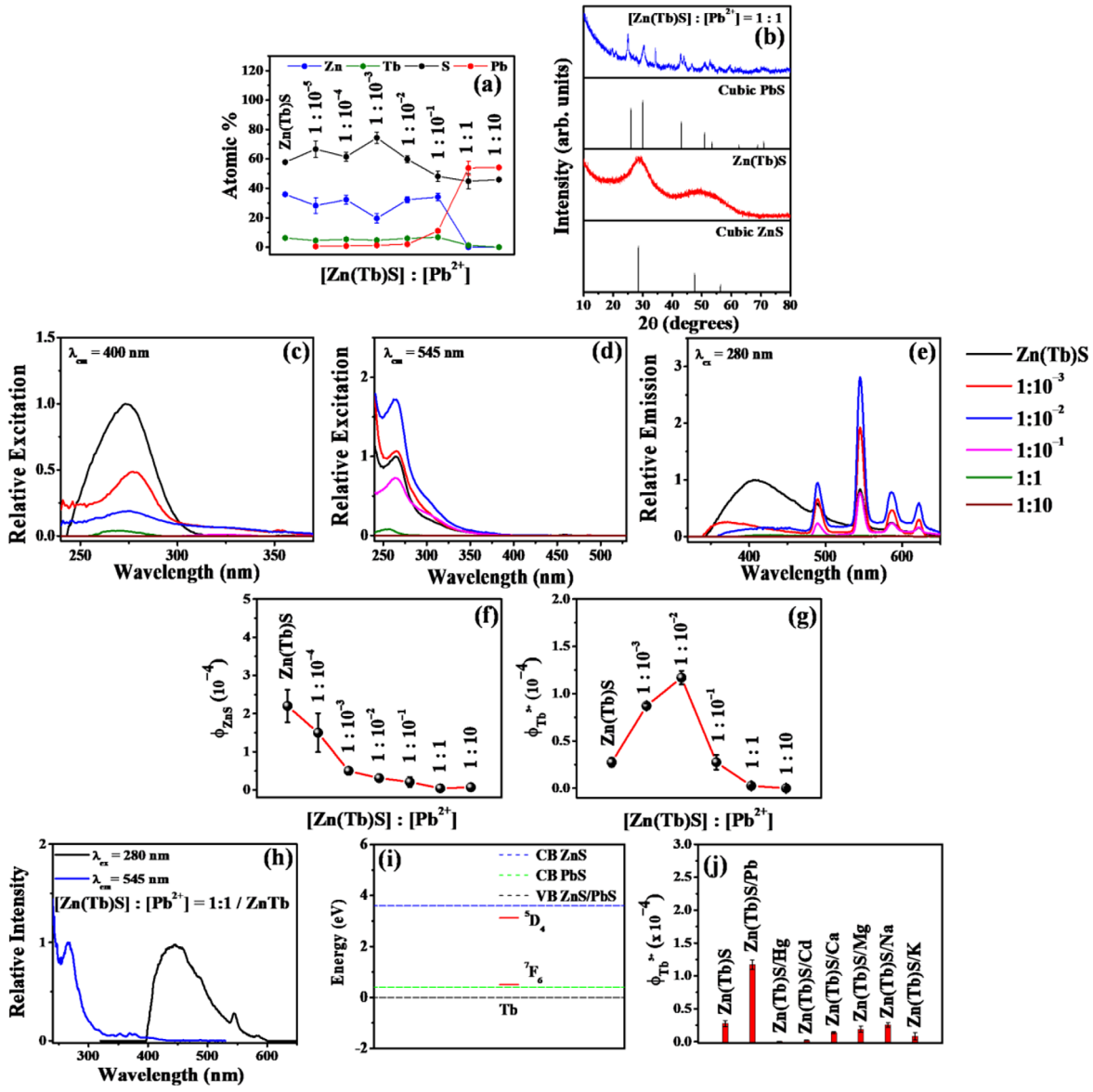

Figure 5. The elemental composition from EDS measurements of the Zn(Tb)S and the Zn(Tb)S NPs that are post-synthetically treated with Pb^{2+} with varying concentrations are shown in panel (a). Panel (b) shows the XRD profiles of the Zn(Tb)S and the NPs with [Zn(Tb)S] : [Pb^{2+}] = 1:1. Panels (c)–(e) show the luminescence excitation and emission spectra of the NPs investigated. The trends in quantum yields of ZnS and Tb^{3+} emissions in the NPs studied are shown in panels (f) and (g), respectively. The luminescence spectra from the experiments when the NPs with [Zn(Tb)S] : [Pb^{2+}] = 1:1 is treated with an excess of Zn^{2+} and Tb^{3+} are shown in panel (h). The relative energy level schematic of Tb^{3+} with respect to the valence and conduction bands of the host ZnS and PbS are shown in panel (i). Panel (j) summarizes the Tb^{3+} emission quantum yields in different Zn(Tb)S/M [M = Pb, Hg, Cd, Ca, Mg, Na, K] NPs, with [Zn(Tb)S] : [M^{n+}] = 1:10^{-2}. (Adapted with permission from Reference [102], Copyright 2018 Royal Society of Chemistry).

reduced efficiency of Tb^{3+} emission in the recovered NPs. Clearly the synthesized Zn(Tb)S NPs and post-synthetically recovered Zn(Tb)S NPs differ in the surface state composition which could have implications in their emission characteristics.

The electronic properties need to be evaluated to understand the completely diminished Tb^{3+} emission in the NPs [Zn(Tb)S]:[Pb^{2+}] ≥ 1:1. In this reaction domain PbS phases form by exchanging Zn^{2+} and to some extent Tb^{3+} from the Zn(Tb)S NPs by Pb^{2+}. PbS has a smaller band gap. The relative energy level positions of Tb^{3+} energy levels in ZnS and PbS are shown in panel (i) of Figure 5. This reveals that the trapping of photogenerated charge carriers is not efficient in PbS, especially the luminescent energy level $^5D_4$ would suffer from auto-ionization even if this energy level is populated by some means. Consequently, Tb^{3+} emission in PbS is highly quenched.

A remarkable outcome from the Pb^{2+} added Zn(Tb)S NPs is the Pb induced Tb^{3+} emission brightening. This is interesting considering the difficulty to make Ln^{3+} luminophores brighter that is associated with very low direct absorption efficiency and quenching of their emission by

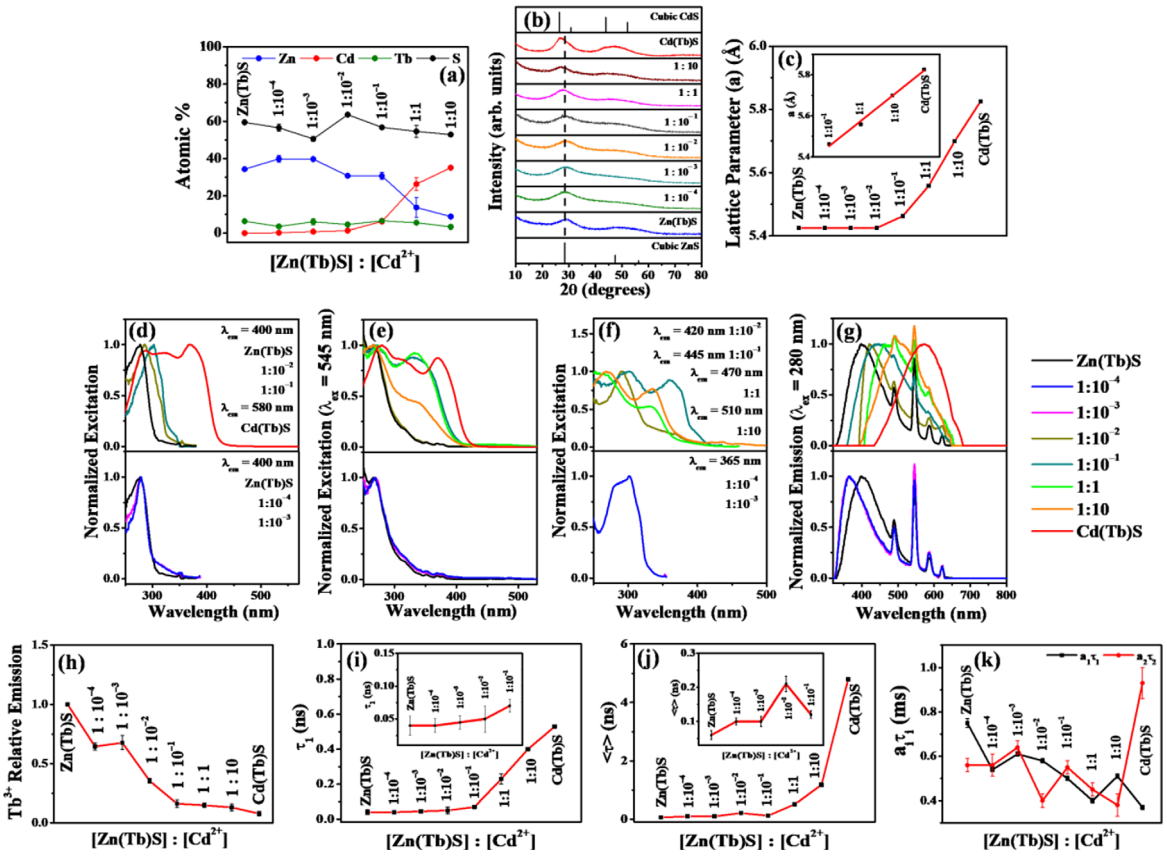

Figure 6. The elemental composition and XRD profiles of the Zn(Tb)S and the Zn(Tb)S NPs that are post-synthetically modified by varying concentrations of Cd^{2+} are shown in panels (a) and (b), respectively. Panel (b) also includes the XRD profile for the Cd(Tb)S NPs. The trend of lattice parameters as a function of composition of the NPs is shown in panel (c). Panels (d) – (g) summarize the luminescence excitation and emission spectra. The trend in Tb^{3+} emission quantum yield is shown in panel (h). Panels (i) and (j) summarize the trends in shorter lifetime component and average lifetime of the broad emission. Panel (k) shows the relative contributions of shorter-lived surface related and longer-lived core related Tb^{3+} emission components in these NPs. (Adapted with permission from Reference [105], Copyright 2019 American Chemical Society).

the vibrational overtones of the immediate ligand and solvent molecules. In order to evaluate the specificity, experiments are performed in which the Zn(Tb)S NPs are post-synthetically treated with various other cations (M^{n+}) with [Zn(Tb)S]:[M^{n+}] = $1{:}10^{-2}$ [M = Hg, Cd, Ca, Mg, Na, K]. The trend in Tb^{3+} emissions from these experiments is shown in panel (j) of Figure 5. A Pb specificity is indeed observed, at least among the cations considered, as the other cations do not provide any such favourable mechanism for Tb^{3+} emission enhancement in the Zn(Tb)S NPs.

(2) Zn(Tb)S/Cd NPs. Cd^{2+} is able to exchange Zn^{2+} from ZnS based nanomaterials and this reaction progression can access the visible spectral window. [103, 104] We undertook experiments in which the Zn(Tb)S NPs are post-synthetically modified by varying concentrations of Cd^{2+} with [Zn(Tb)S]:[Cd^{2+}] = $1{:}10^{-4}$–1:10 [105]. Similar to the concept discussed for the Pb^{2+} treated Zn(Tb)S NPs discussed above, these experiments also cover the pre-cation exchange and cation exchanged NPs. One of the prime objective of this work is to investigate how the structural evolution of the NPs can tune the emission properties of the dopant Tb^{3+} in the Zn(Tb)S NPs.

The elemental composition of the Zn(Tb)S NPs and the NPs with [Zn(Tb)S]:[Cd^{2+}] = $1{:}10^{-4}$–1:10 are shown in panel (a) of Figure 6. The amounts of Zn, Tb, and S remains almost similar in the range of [Zn(Tb)S]:[Cd^{2+}] = $1{:}10^{-4}$–$1{:}10^{-2}$, with the incorporation of Cd in the NPs being evident. Further increase of [Cd^{2+}] gradually displaces Zn^{2+} from the NPs and a partial cation exchange proceeds. Even in presence of an excess amount of Cd^{2+}, under the reaction condition the exchange of Zn^{2+} by post-synthetically treated Cd^{2+} remains partial. Others researchers also have discussed such a partial cation exchange for Zn^{2+}–Cd^{2+} combination [106]. It is important that throughout the reaction, the amount of Tb in the NPs remains similar. That is, exchange of Tb^{3+} by Cd^{2+} is not happening. Thus, these NPs can directly monitor the impact on Tb^{3+} emission that may arise from the NP's structural changes. The XRD profiles can track the reaction progression, as shown in panel (b) of Figure 6, indicates formation of characteristic cubic crystal phases for both the Zn(Tb)S and partially exchanged NPs. It is to note that the XRD peak positions in the NPs with [Zn(Tb)S]:[Cd^{2+}] = 1:1/1:10 does not match completely

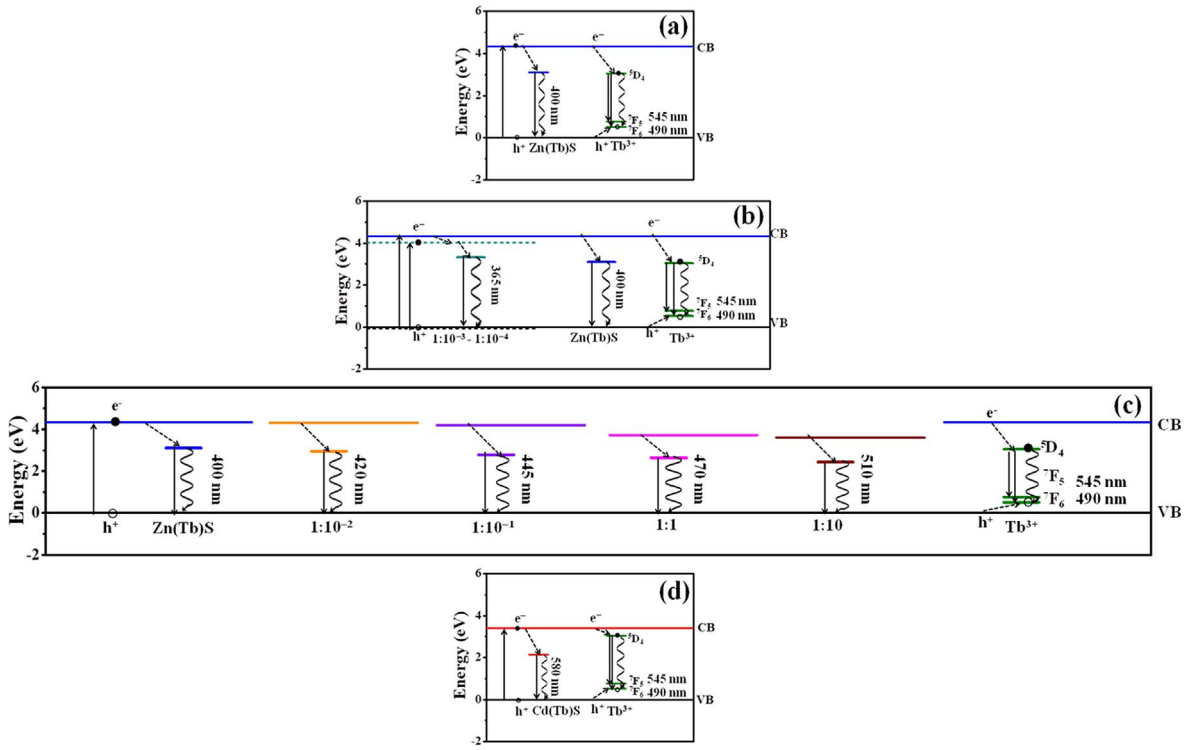

Figure 7. The relative energy level that positions the Tb^{3+} energy levels with respect to the valence and conduction bands of the Zn(Tb)S NPs, the NPs with [Zn(Tb)S] : $[Cd^{2+}] = 1{:}10^{-4}$–$1{:}10^{-3}$, the NPs with [Zn(Tb)S]:$[Cd^{2+}] = 1{:}10^{-2}$–1:10, and the Cd(Tb)S NPs are shown in panels (a)–(d), respectively. (Adapted with permission from Reference [105], Copyright 2019 American Chemical Society).

with the corresponding profile of the Cd(Tb)S NPs. This further corroborates with a partial cation exchange. The unit cell parameters of the different NPs investigated are plotted as a function of composition of the NPs, and are shown in panel (c) of Figure 6. The Vegard law analysis reveals a linear trend, suggesting formation of homogeneous alloy while the Zn(Tb)S NPs are post-synthetically treated with Cd^{2+}. Cd^{2+} addition to the Zn(Tb)S NPs with 3.0 ± 0.6 nm diameter and the NPs with [Zn(Tb)S]:$[Cd^{2+}] = 1{:}1$ produces particles with 3.1 ± 0.6 nm diameter, suggesting no significant alteration of the NP's dimension following the post-synthetic reaction.

The luminescence spectra of the Zn(Tb)S NPs and the post-synthetically modified NPs are shown in panels (d)–(g) of Figure 6. In presence of very low $[Cd^{2+}]$ in the NPs with [Zn(Tb)S]:$[Cd^{2+}] = 1{:}10^{-4}$–$1{:}10^{-3}$, emission band maxima blue shifts. This suggests significant reorganization of surface trap states can occur even in presence of small amount of Cd in the NPs. Once the reactant concentration ratio reaches [Zn(Tb)S]:$[Cd^{2+}] = 1{:}10^{-2}$, NP's band gap starts decreasing. The emission band maxima thus red shifts. Emissions from these NPs span the UV–visible spectral window. The excitation spectra also reveal this composition change of the NPs with characteristic spectral shift. Monitoring the Tb^{3+} emission band at 545 nm reveal an excitation spectrum that is broad and devoid of sharp direct excitation bands indicative of host sensitized dopant emission. The Tb^{3+} emission quantum yield trend, as shown in panel (h) of Figure 6, shows a decrease in the NPs with [Zn(Tb)S]:$[Cd^{2+}] = 1{:}10^{-4}$–$1{:}10^{-3}$. This decrease suggests that minor alterations in NP's surface state composition can affect the Tb^{3+} emission in these NPs. Further decrease of Tb^{3+} emission quantum yield in the NPs with [Zn(Tb)S]:$[Cd^{2+}] = 1{:}10^{-2}$–1:10 reflects the formation of Zn–Cd alloyed NPs (*vide infra*).

Measurements of emission lifetimes provide information on corresponding rates of reactions. There are two emissive centers in Zn(Tb)S, the broad ZnS and sharp Tb^{3+} emission bands. In order to address how the dynamics proceed, the emission lifetimes of both these bands were collected in the Zn(Tb)S and Zn(Tb)S/Cd NPs. The trends in shorter lifetime component and average lifetime from the shorter-lived ZnS emission lifetime measurements are summarized in panels (i) and (j), respectively. A salient feature from the emission lifetimes of the broad band include $[Cd^{2+}]$ dependent depopulation kinetics in the NPs with a lengthening with gradual progression of cation exchange. The trend in contributions from shorter-lived surface related and longer-lived core related lifetime components of Tb^{3+} emission is shown in panel (k) of Figure 6. Tracking Tb^{3+} kinetics directly captures significant reorganization in the NP's surface states, as evidenced by a decrease in the contribution of the shorter lifetime component.

In order to rationalize the photophysical outcomes in the NPs investigated, the relative energy levels that place

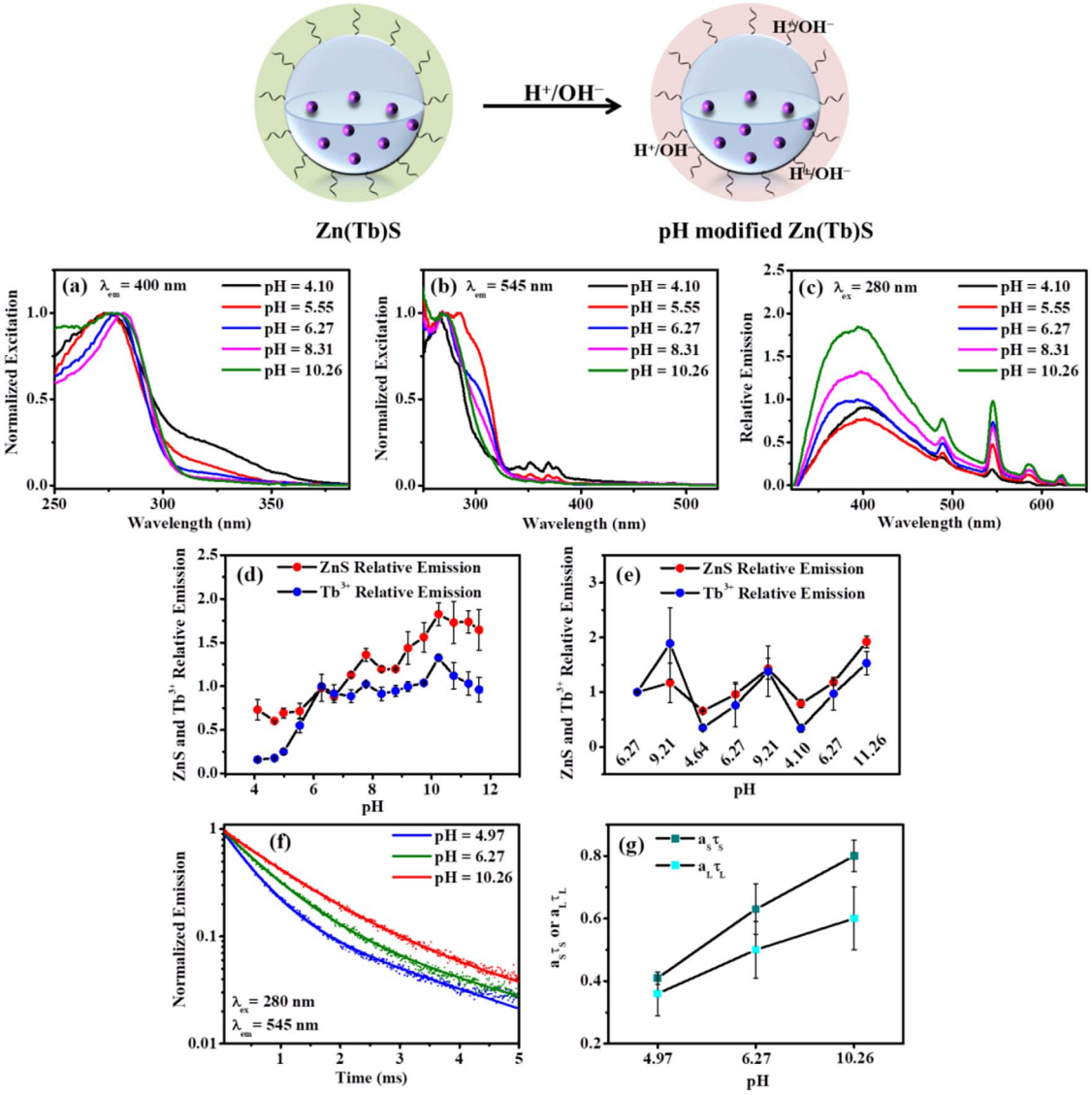

Figure 8. The luminescence excitation and emission spectra of the Zn(Tb)S NPs as a function of pH that is modified post-synthetically are shown in panels (a)–(c), respectively. Panel (d) summarizes the relative trend of ZnS and Tb^{3+} emissions in these NPs. The reversible nature of pH dependent effect is shown in panel (e). Panels (f) and (g) show the Tb^{3+} emission lifetime decay profiles and the trends of contributions from shorter-lived surface related and longer-lived core related lifetime components. (Adapted with permission from Reference [108], Copyright 2020 American Chemical Society).

the dopant Tb^{3+} energy levels with respect to the valence and conduction bands of the host material are constructed, and these are shown in Figure 7. In the Zn(Tb)S NPs, Tb^{3+} ground and luminescent energy levels are suitably placed above and below the valence and conduction bands of the host ZnS, and hence these energy levels can act as hole and electron traps. Subsequent electron-hole pair recombination at these Tb^{3+} related trap sites populates the Tb^{3+} luminescent energy levels, thus generating the ZnS NP host sensitized dopant Tb^{3+} emission from the Zn (Tb)S NPs. In the NPs with [Zn(Tb)S]:[Cd^{2+}] = $1:10^{-4}$–$1:10^{-3}$, the Cd only acts as a surface state modulator and dopant moiety. Presence of Cd in ZnS shift the valence and conduction bands by 0.08 and 0.32 eV below their original positions [107]. This can be correlated with observation of an additional band at 305 nm in the luminescence excitation spectrum while monitoring the 365 nm emission of these NPs. Furthermore, shifting of the conduction band can increase the probability of back electron transfer and thus reduce the Tb^{3+} emission quantum yield. Formation of the alloyed $Zn_{1-x}Cd_xS$ in the NPs with [Zn(Tb)S]:[Cd^{2+}] = $1:10^{-2}$–1:10 while extends the Tb^{3+} excitation to lower energy, they yield Tb^{3+} emission to a lesser extent. In these NPs, the band gaps gradually decrease. Thus, in the alloys with gradual exchange of Zn^{2+} by Cd^{2+}, the ΔE_2 value gradually decreases. This results in roles of auto-ionization of excited electrons in the Tb^{3+} energy level more facile, thus decreasing their emission. Finally, in the Cd(Tb)S NPs this effect is even more enhanced and the Tb^{3+} emission is reduced.

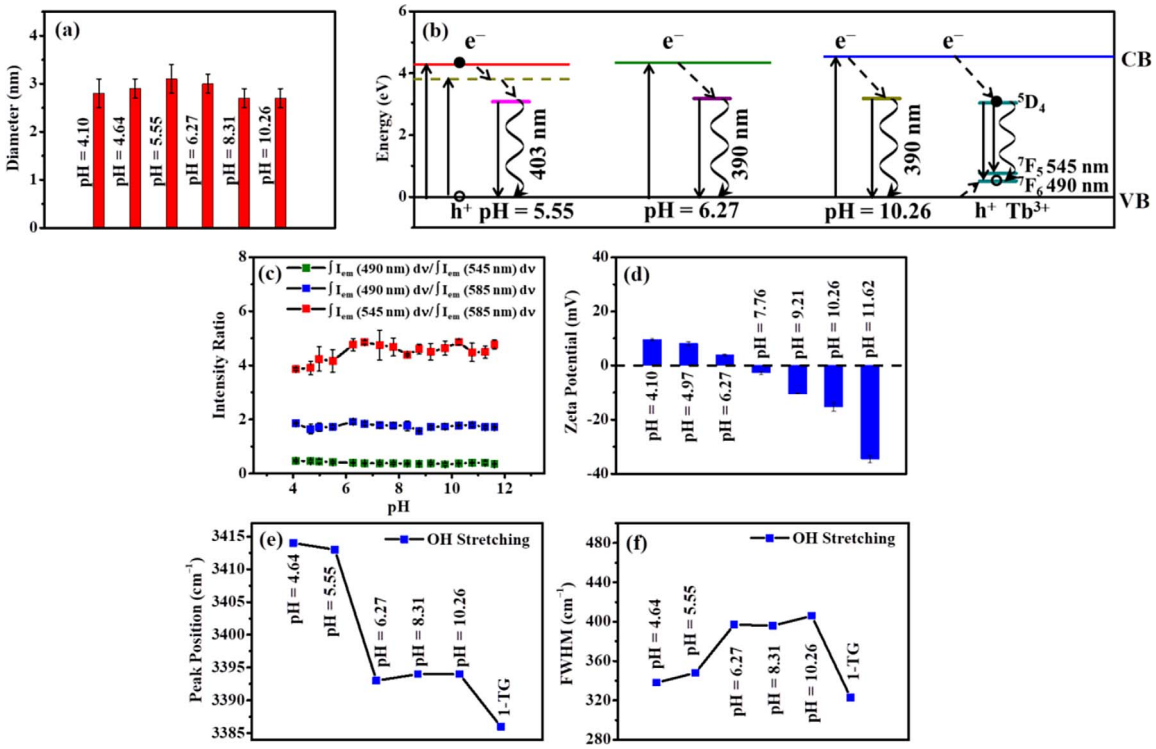

Figure 9. The size of the Zn(Tb)S NPs as a function of pH that is adjusted post-synthetically is shown in panel (a). Panel (b) shows the relative energy level schematic of the Zn(Tb)S NPs in different pH. A comparison of Tb^{3+} emission spectral shape is shown in panel (c). The zeta potential values, and the trends in spectral characteristics of OH stretching absorption band are shown in panels (d) and (e) - (f), respectively. (Adapted with permission from Reference [108], Copyright 2020 American Chemical Society).

B. Zn(Tb)S NPs : Surface Alteration. The experiments discussed above demonstrate the usefulness of post-synthetic reaction strategy to generate Ln doped inorganic NPs and ways to tune their electronic properties. These systems essentially change the NP's core structure. Another extremely important variable in the quantum confined regime is the NP's surface state composition. This surface has two components in the form of surface localized atoms and the surface capping ligands. A suitable capping on the NPs confers stability and guides its dispersion nature. In a series of experiments with 1-TG capped Zn(Ln)S [Ln = Sm, Eu, Tb, Dy] NPs, we identified that this ligand offers aqueous dispersion of the NPs and Zn(Tb)S NPs as the most efficient system with host sensitized Tb^{3+} emission [86]. Correspondingly, it remains elusive to decipher the effect of 1-TG structural alteration on the luminescence behavior of the NPs. This aspect is addressed by performing experiments in which the pH of the aqueous dispersion of the 1-TG capped Zn(Tb)S NPs was controlled post-synthetically. [108] By virtue of the fact 1-TG has ionizable groups; a change in pH of the medium should modify its chemical identity [109].

Panels (a)–(c) of Figure 8 show the luminescence excitation and emission spectra of the Zn(Tb)S NPs as a function of pH that has been adjusted post-synthetically. All the NPs show characteristic broad blue ZnS emission and sharp Tb^{3+} emission bands. Excitation spectra, while monitoring the Tb^{3+} emission at 545 nm, reveal a broad profile with significant overlap to that obtained while monitoring the ZnS centered emission band at 400 nm, suggesting that operation of host sensitization is present in all these NPs. However, the extent of ZnS and Tb^{3+} emissions is clearly different. These trends are shown in panel (d) of Figure 8. Both of these emissions increase with an increase in pH of the medium, with the effect being more prominent in the Tb^{3+} emission. In this line, it is observed that the proportion of direct excitation over host sensitization for Tb^{3+} emission increases in acidic pH. Furthermore, this pH dependent tuning of emission is found to be reversible, as shown in panel (e) of Figure 8. This suggests an importance of structural alterations of surface capping ligand in guiding the observed trend in photophysical properties and that this is not a mere reflection of NP's surface photochemistry. The Tb^{3+} emission lifetime decay profiles at different pH of the dispersion are shown in panel (f) of Figure 8. Corresponding contributions from individual lifetime components are shown in panel (g) of Figure 8. There is a lengthening of emission lifetime on going from acidic to basic pH. Closer inspection reveals that this effect is specific for the shorter surface related lifetime component on going from pH 4.97 to 6.27, while the other changes show a general effect. Thus, these results clearly demonstrate that the Tb^{3+} emission properties are guided by the alterations in the surface state composition of the NPs.

In order to understand the trend in Tb^{3+} emission in these NPs, effects of band alignment, dopant local site

symmetry, and capping ligand structural alterations are systematically evaluated. The size of the NPs and the corresponding relative energetic, Tb^{3+} emission spectral shape, zeta potential, and IR absorption spectral characteristic of OH stretching band are shown in panels (a)–(b), (c), (d), and (e)–(f) of Figure 9, respectively. The post-synthetic modification of NPs does not result in significant changes in NP dimension and dramatic alterations in Tb^{3+} emission band shapes; indicating that the changes in the relative band alignment and coordination environment are not the governing factors and subtle modifications in the ligand structure is primarily responsible in dictating the photophysical outcome in these NPs. This change can be visualized by zeta potential measurements and in the infrared absorption spectral features. Additionally, a decrease in Tb content in the NPs is observed in acidic medium, as evaluated by the EDS measurements. These analyses strongly suggest that post-synthetic modification of inorganic NPs also has the ability to control dopant emission by altering surface capping ligand structure, even when the NP's core related variables are relatively unperturbed.

Conclusions

Motivated by the unprecedented opportunity of post-synthetic modification of inorganic NPs and the luminescence properties of Ln^{3+}, this work summarizes the key outcomes from experiments in which either the semiconductor NPs are treated post-synthetically with Ln^{3+} from solutions or the synthetically Ln^{3+} incorporated (doped) semiconductor NPs are treated post-synthetically by other cations from solutions. Treating ZnS/CdS/CdSe NPs with Ln^{3+} at room temperature incorporates Ln in the NPs in all cases and in the ZnS/Ln [Ln = Eu, Tb, Yb], CdS/Ln [Ln = Eu, Tb], and CdSe/Ln [Ln = Eu, Tb] host sensitized Ln^{3+} emission is realized. These observations can be well rationalized by a charge trapping mediated dopant emission sensitization mechanism. In this model, the Ln^{3+} ground and luminescent energy levels need to be optimally placed with respect to the valence and conduction bands of the host NP, thus they can act as the charge trap centers for the photogenerated hole and electron pairs. The electron-hole pair recombination at the Ln^{3+} related trap sites populates the Ln^{3+} luminescent energy levels, thus generating the optical antenna effect with NPs sensitized Ln^{3+} emission. While post-synthetically modifying the Zn(Tb)S NPs with Pb^{2+} / Cd^{2+}, two relative reactant concentration regimes are investigated. These are [Zn(Tb)S]:[Pb^{2+}]/[Cd^{2+}] = $1:10^{-4}$–$1:10^{-2}$ and $1:10^{-2}$–1:10, which represent pre-cation and cation exchanged NPs, respectively. Remarkably existence of rich photophysics are observed in both the cases, with a Pb specific Tb^{3+} emission brightening in the NPs with [Zn(Tb)S]:[Pb^{2+}] = $1:10^{-3}$–$1:10^{-2}$. This observation finds a global interest in the light of brightening an Ln^{3+} luminophore in general, that is interesting due to inefficient direct excitation and environment induced Ln^{3+} emission quenching. In the cation exchanged reaction conditions, it is observed that under the reaction conditions employed Pb^{2+} and Cd^{2+} can completely and partially exchange Zn^{2+} from the Zn(Tb)S NPs, respectively. In Zn(Tb)S/Pb NPs, a decrease in Tb content is also observed, an effect which is found to be absent in the Zn(Tb)S/Cd NPs. Photophysical properties in these NPs can be well tracked with the change in the NPs band gap and the charge trapping mediated processes. Experiments are also performed with the post-synthetically pH modified 1-TG capped Zn(Tb)S NPs. These measurements reveal a dramatic effect of capping ligand structure in controlling both the ZnS and Tb^{3+} emissions reversibly. Systematic analysis reveals that in this process the effects of band gap engineering and drastic modification of dopant local site symmetry is not important, further emphasizing the control from the capping ligand structure.

In short, the results discussed demonstrate that it is possible to generate Ln^{3+} semiconductor NPs based luminophores by using the post-synthetic modification strategy, and the electronic properties of Ln^{3+} centers in the Ln^{3+} doped semiconductor NPs can also be modified by post-synthetic addition of other cations, by either modulating their core or surface structure. Future directions in this research field include development of co-doped NPs and engineering the surface of the NPs for potential multiplex assays and targeted therapy.

Acknowledgments

Financial supports from the Science and Engineering Research Board (SERB), Department of Science and Technology (DST) (SB/S1/PC-040/2013) and the University Grants Commission (UGC)(F. 20-11 (17)/2013(BSR)), India are acknowledged. Saoni Rudra and Madhumita Bhar acknowledge fellowship support from the University of Calcutta and the Council of Scientific and Industrial Research (CSIR), respectively. We also acknowledge the support from CRNN, University of Calcutta. Prasun Mukherjee also acknowledges Dr. Gouranga H. Debnath, Ms. Saoni Rudra, Ms. Madhumita Bhar, Dr. Chad M. Shade, Dr. Daniel N. Lamont, Ms. Robin F. Sloan who have contributed in this project. Prasun Mukherjee sincerely thanks Prof. Stéphane Petoud and Prof. David H. Waldeck for introducing him to the lanthanide-semiconductor NPs project and for many insightful discussions.

References

1. Steigerwald ML, Alivisatos AP, Gibson JM, Harris TD, Kortan R, Muller AJ, Thayer AM, Duncan TM, Douglass DC, Brus LE (1988), Surface derivatization and isolation of semiconductor cluster molecules. J. Am. Chem. Soc. 110, 3046–3050.
2. Murray CB, Norris DJ, Bawendi MG (1993), Synthesis and characterization of nearly monodisperse CdE (E = Sulfur, Selenium, Tellurium) semiconductor nanocrystallites. J. Am. Chem. Soc. 115, 8706–8715.

3. Park J, Joo J, Kwon SG, Jang Y, Hyeon T (2007), Synthesis of monodisperse spherical nanocrystals. Angew. Chem. Int. Ed. 46, 4630–4660.
4. van Embden J, Jasieniak JJ (2015), The heat-up synthesis of colloidal nanocrystals. Chem. Mater. 27, 2246–2285.
5. Luo W, Li R, Liu G, Antonio MR, Chen X (2008), Evidence of trivalent europium incorporated in anatase TiO_2 nanocrystals with multiple sites. J. Phys. Chem. C 112, 10370–10377.
6. Luo W, Li R, Chen X (2009), Host-sensitized luminescence of Nd^{3+} and Sm^{3+} ions incorporated in anatase titania nanocrystals J. Phys. Chem. C 113, 8772–8777.
7. Son DH, Hughes SM, Yin Y, Alivisatos AP (2004), Cation exchange reactions in ionic nanocrystals. Science 306, 1009–1012.
8. Robinson RD, Sadtler B, Demchenko DO, Erdonmez CK, Wang L-W, Alivisatos AP (2007), Spontaneous superlattice formation in nanorods through partial cation exchange. Science 317, 355–358.
9. Sadtler B, Demchenko DO, Zheng H, Hughes SM, Merkle MG, Dahmen U, Wang L-W, Alivisatos AP (2009), Selective facet reactivity during cation exchange in cadmium sulfide nanorods. J. Am. Chem. Soc. 131, 5285–5293.
10. Jain PK, Amirav L, Aloni S, Alivisatos AP (2010), Nanoheterostructure cation exchange: anionic framework conservation. J. Am. Chem. Soc. 132, 9997–9999.
11. Beberwyck BJ, Alivisatos AP (2012), Ion exchange synthesis of III−V nanocrystals. j. Am. Chem. Soc. 134, 19977–19980.
12. Miszta K, Dorfs D, Genovese A, Kim MR, Manna L (2011), Cation exchange reactions in colloidal branched nanocrystals. ACS Nano 5, 7176–7183.
13. Li H, Zanella M, Genovese A, Povia M, Falqui A, Giannini C, Manna L (2011), Sequential cation exchange in nanocrystals: preservation of crystal phase and formation of metastable phases. Nano Lett. 11, 4964–4970.
14. Lesnyak V, George C, Genovese A, Prato M, Casu A, Ayyappan S, Scarpellini A, Manna L (2014), Alloyed copper chalcogenide nanoplatelets via partial cation exchange reactions. ACS Nano 8, 8407–8418.
15. Trizio LD, Li H, Casu A, Genovese A, Sathya A, Messina GC, Manna L (2014), Sn cation valency dependence in cation exchange reactions involving $Cu_{2-x}Se$ NANOCRYSTALS. J. Am. Chem. Soc. 136, 16277–16284.
16. Li H, Brescia R, Povia M, Prato M, Bertoni G, Manna L, Moreels I (2013), Synthesis of uniform disk-shaped copper telluride nanocrystals and cation exchange to cadmium telluride quantum disks with stable red emission. J. Am. Chem. Soc. 135, 12270–12278.
17. Khan AH, Pinchetti V, Tanghe I, Dang Z, Martín-García B, Hens Z, Thourhout DV, Geiregat P, Brovelli S, Moreels I (2019), Tunable and efficient red to near-infrared photoluminescence by synergistic exploitation of core and surface silver doping of CdSe nanoplatelets. chem. Mater. 31, 1450–1459.
18. Mocatta D, Cohen G, Schattner J, Millo O, Rabani E, Banin U (2011), Heavily doped semiconductor nanocrystal quantum dots. Science 332, 77–81.
19. Sahu A, Kang MS, Kompch A, Notthoff C, Wills AW, Deng D, Winterer M, Frisbie CD, Norris DJ (2012), Electronic impurity doping in CdSe NANOCRYSTALS. NANO Lett. 12, 2587–2594.
20. Dong C, van Veggel FCJM (2009), Cation exchange in lanthanide fluoride nanoparticles. ACS Nano 3, 123–130.
21. Beberwyck BJ, Surendranath Y, Alivisatos AP (2013), Cation exchange: a versatile tool for nanomaterials synthesis. J. Phys. Chem. C 117, 19759–19770.
22. Rivest JB, Jain PK (2013), Cation exchange on the nanoscale: an emerging technique for new material synthesis, device fabrication, and chemical sensing. Chem. Soc. Rev. 42, 89–96.
23. Trizio LD, Manna L (2016), Forging colloidal nanostructures via cation exchange reactions. Chem. Rev. 116, 10852–10887.
24. Zhang J, Di Q, Liu J, Bai B, Liu J, Xu M, Liu J (2017), Heterovalent doping in colloidal semiconductor nanocrystals: cation-exchange-enabled new accesses to tuning dopant luminescence and electronic impurities. J. Phys. Chem. Lett. 8, 4943–4953.
25. Cho G, Park Y, Hong Y-K, Ha D-H (2019), Ion exchange: an advanced synthetic method for complex nanoparticles. Nano Convergence 6, 17.
26. Li X, Ji M, Li H, Wang H, Xu M, Rong H, Wei J, Liu J, Liu J, Chen W, Zhu C, Wang J, Zhang J (2020), Cation/anion exchange reactions toward the syntheses of upgraded nanostructures: principles and applications. Matter 2, 554–586.
27. Sooklal K, Cullum BS, Angel SM, Murphy CJ (1996), Photophysical properties of ZnS nanoclusters with spatially localized Mn^{2+} J. Phys. Chem. 100, 4551–4555.
28. Isarov AV, Chrysochoos J (1997), Optical and photochemical properties of nonstoichiometric cadmium sulfide nanoparticles: surface modification with copper (II) Ions. Langmuir 13, 3142–3149.
29. Bhargava RN, Gallagher D, Hong X, Nurmikko A (1994), Optical properties of manganese-doped nanocrystals of ZnS. Phys. Rev. Lett. 72, 416–419.
30. Bhargava RN (1996), Doped Nanocrystalline materials – physics and applications. J. Lumin. 70, 85–94.
31. Richardson FS (1982), Terbium (III) and europium (III) ions as luminescent probes and stains for biomolecular systems. Chem. Rev. 82, 541–552.
32. Bünzli J-CG, Piguet C (2005), Taking advantage of luminescent lanthanide ions. Chem. Soc. Rev. 34, 1048–1077.
33. Eliseeva SV, Bünzli J-CG (2010), Lanthanide luminescence for functional materials and bio-sciences. Chem. Soc. Rev. 39, 189–227.
34. Bünzli J-CG (2010), Lanthanide luminescence for biomedical analyses and imaging. Chem. Rev. 110, 2729–2755.
35. Moore EG, Samuel APS, Raymond KN (2009), From antenna to assay: lessons learned in lanthanide luminescence. Acc. Chem. Res. 42, 542–552.
36. Binnemans K (2009), Lanthanide-based luminescent hybrid materials. Chem. Rev. 109, 4283–4374.
37. Hildebrandt N, Löhmannsröben H-G (2007), Quantum dot nanocrystals and supramolecular lanthanide complexes – energy transfer systems for sensitive *in vitro* diagnostics and high throughput screening in chemical biology. Curr. Chem. Biol. 1, 167–186.
38. Bünzli J-CG (2013), Lighting up cells with lanthanide self-assembled helicates. Interface Focus 3, 20130032.
39. Bünzli J-CG, Eliseeva SV (2010), Lanthanide NIR luminescence for telecommunications, bioanalyses and solar energy conversion. J. Rare Earths 28, 824–842.
40. Thibon A, Pierre VC (2009), Principles of responsive lanthanide-based luminescent probes. Anal. Bioanal. Chem. 394, 107–120.
41. Alcala MA, Kwan SY, Shade CM, Lang M, Uh H, Wang M, Weber SG, Bartlett DL, Petoud S, Lee YJ (2011), Luminescence targeting and imaging using a nanoscale generation 3 dendrimer in an in vivo colorectal metastatic rat model. Nanomedicine: Nanotechnology, Biology, and Medicine 7, 249–258.
42. Foucault-Collet A, Gogick KA, White KA, Villette S, Pallier A, Collet G, Kieda C, Li T, Geib SJ, Rosi NL, Petoud S (2013), Lanthanide near infrared imaging in living

cells with Yb^{3+} nano metal organic frameworks. PNAS 110, 17199–17204.
43. Chen Z, Zheng W, Huang P, Tu D, Zhou S, Huang M, Chen X (2015), Lanthanide-doped luminescent, Nanoscale 2015, 4274–4290.
44. Teo RD, Termini J, Gray HB (2016), Lanthanides: applications in cancer diagnosis and therapy. J. Med. Chem. 59, 6012–6024.
45. Debnath GH, Bhattacharya S, Adhikary A, Mukherjee P (2018), Host-sensitized sharp samarium emission from doped titanium dioxide nanoparticles as non-cytotoxic photostable reporters for live-cell imaging,. New 42, 14832–14842.
46. Beeby A, Clarkson IM, Dickins RS, Faulkner S, Parker D, Royle L, de Sousa AS, Woods M (1999), Non-radiative deactivation of the excited states of europium, terbium and ytterbium complexes by proximate energy-matched OH, NH and CH oscillators: an improved luminescence method for establishing solution hydration states. J. Chem. Soc. Perkin Trans. 2, 493–503.
47. Bünzli J-CG (2015), On the design of highly luminescent lanthanide complexes. Coord. Chem. Rev. 293–294, 19–47.
48. Lemonnier J-F, Guénée L, Beuchat C, Wesolowski TA, Mukherjee P, Waldeck DH, Gogick KA, Petoud S, Piguet C (2011), Optimizing sensitization processes in dinuclear luminescent lanthanide oligomers: selection of rigid aromatic spacers. J. Am. Chem. Soc. 133, 16219–16234.
49. Lemonnier J-F, Babel L, Guénée L, Mukherjee P, Waldeck DH, Eliseeva SV, Petoud S, Piguet C (2012), Perfluorinated aromatic spacers for sensitizing Europium (III) centers in dinuclear oligomers: Better than the best by chemical design? Angew. Chem. Int. Ed. 51, 11302–11305.
50. Aboshyan-Sorgho L, Nozary H, Aebischer A, Bünzli J-CG, Morgantini P-Y, Kittilstved KR, Hauser A, Eliseeva SV, Petoud S, Piguet C (2012), Optimizing millisecond time scale near-infrared emission in polynuclear chrome (III)−lanthanide (III) complexes. J. Am. Chem. Soc. 134, 12675–12684.
51. Manna P, Bhar M, Mukherjee P (2021), Lanthanide photoluminescence lifetimes reflect vibrational signature of local environment: lengthening duration of emission in inorganic nanoparticles. J. Luminescence 235, 118052.
52. Bol AA (2002), On the incorporation of trivalent rare earth ions in II-VI semiconductor. Nanocrystals Chem. Mater. 14, 1121–1126.
53. Chengelis DA (2005), Incorporating lanthanide cations with cadmium selenide nanocrystals: a strategy to sensitize and protect Tb(III). J. Am. Chem. Soc. 127, 16752–16753.
54. Chen X, Luo W, Liu Y, Liu G (2007), Recent progress on spectroscopy of lanthanide ions incorporated in semiconductor. Nanocrystals J. Rare Earths 25, 515–525.
55. Luo W, Liu Y, Chen X (2015), Lanthanide-doped, Sci. China Mat. 58, 819–850
56. Chen D, Wang Y (2013), Impurity doping: a novel strategy for controllable synthesis of functional lanthanide nanomaterials. Nanoscale 5, 4621–4637.
57. Wang G, Peng Q, Li Y (2011), Lanthanide-doped nanocrystals: synthesis, optical-magnetic properties, and applications. Acc. Chem. Res. 44, 322–332.
58. Chen P, Zhang J, Xu B, Sang X, Chen W, Liu X, Han J, Qiu J (2014), Lanthanide doped nanoparticles as remote sensors for magnetic fields. Nanoscale 6, 11002–11006.
59. Pan G, Bai X, Yang D, Chen X, Jing P, Qu S, Zhang L, Zhou D, Zhu J, Xu W, Dong B, Song H (2017), Doping lanthanide into perovskite nanocrystals: highly improved and expanded optical properties. Nano Lett. 17, 8005–8011.
60. Debnath GH, Bloom BP, Tan S, Waldeck DH (2022), Room temperature doping of Ln^{3+} in perovskite nanoparticles: a halide exchange mediated cation exchange approach Nanoscale 14, 6037–6051.
61. Kong J, Zhu H, Li R, Luo W, Chen X (2009), Carrier-mediated 1.55 mm photoluminescence from Single Er^{3+} center in SnO_2 NANOCRYSTALS OPTICS Lettters 34, 1873–1875.
62. Kong J, Zheng W, Liu Y, Li R, Ma E, Zhu H, Chen X (2015), Persistent luminescence from Eu^{3+} in SnO_2 nanoparticles Nanoscale 7, 11048–11054.
63. Luo W, Fu C, Li R, Liu Y, Zhu H, Chen X (2011), Er^{3+} - doped anatase TiO_2 nanocrystals: crystal-field levels, excited-state dynamics, upconversion, and defect luminescence Small 7, 3046–3056.
64. Chen L, Zhang J, Lu S, Ren X, Wang X (2005), On the energy transfer from nanocrystalline ZnS to Tb^{3+} ions confined in reverse micelles Chem. Phys. Lett. 409, 144–148.
65. Jing-hua N, Rui-nian H, Wen-lian L, Ming-tao L, Tian-zhi Y (2006), Electroluminescent properties of a device based on terbium-doped ZnS nanocrystals. J. Phys. D: Appl. Phys. 39, 2357–2360.
66. Planelles-Aragó J, Julián-López B, Cordoncillo E, Escribano P, Pellé F, Viana B, Sanchez C (2008), Lanthanide doped ZnS quantum dots dispersed in silica glasses: an easy one pot sol-gel synthesis for obtaining novel photonic materials. J. Mater. Chem. 18, 5193–5199.
67. Ehrhart G, Capoen B, Robbe O, Beclin F, Boy P, Turrell S, Bouazaoui M (2008), Energy transfer between semiconductor nanoparticles (ZnS or CdS) and Eu^{3+} ions in sol-gel derived ZrO_2 thin films Optical Materials 30, 1595–1602.
68. Dong L, Liu Y, Zhuo Y, Chu Y (2010), General Route to the Fabrication of ZnS and M-Doped (M = Cd^{2+}, Mn^{2+}, Co^{2+}, Ni^{2+}, and Eu^{3+}) ZnS Nanoclews and a Study of Their Properties Eur. J. Inorg. Chem. 2010, 2504–2513.
69. Hou S, Yuen Y, Mao H, Wang J, Zhu Z (2009), Photoluminescence properties of the Eu^{3+}-doped ZnS nanocrystals and the crystal-field analysis J. Phys. D: Appl. Phys. 42, 215105 (5 pp).
70. Qu SC, Zhou WH, Liu FQ, Chen NF, Wang ZG, Pan HY, Yu DP (2002), Photoluminescence Properties of Eu^{3+}-Doped ZnS Nanocrystals Prepared in a Water/Methanol Solution Appl. Phys. Lett. 80, 3605–3607.
71. Sun XL, Zhang GL, Tang GQ, Chen WJ (1999), The site symmetry of Eu^{3+} in ZnS:Eu nanoparticle Chin. Chem. Lett. 10, 807–810.
72. Sun L, Yan C, Liu C, Liao C, Li D, Yu J (1998), Study of the optical properties of Eu^{3+}-doped ZnS nanocrystals J. Alloys Compounds 275–277, 234–237.
73. Wang L, Xu X, Yuan X (2010), Preparation and photoluminescent properties of doped nanoparticles of ZnS by solid-state reaction. J. Lumin. 130, 137–140.
74. Yang H, Yu L, Shen L, Wang L (2004), Preparation and luminescent properties of Eu^{3+}-doped zinc sulfide nanocrystals Mater. Lett. 58, 1172–1175.
75. Planelles-Aragó J, Cordoncillo E, Ferreira RAS, Carlos LD, Escribano P (2011), Synthesis, Characterization and optical studies on lanthanide-doped CdS quantum dots: new insights on CdS/lanthanide energy transfer mechanisms. J. Mater. Chem. 21, 1162–1170.
76. Dethlefsen JR, Mikhailovsky AA, Burks PT, Døssing A, Ford PC (2012), Lanthanide modification of CdSe/ZnS core/shell quantum dots. J. Phys. Chem. C 116, 23713–23720.
77. Martín-Rodríguez R, Geitenbeek R, Meijerink A (2013), Incorporation and luminescence of Yb^{3+} in CdSe nanocrystals J. Am. Chem. Soc. 135, 13668–13671.

78. Mukherjee P, Shade CM, Yingling AM, Lamont DN, Waldeck DH, Petoud S (2011), Lanthanide sensitization in II-VI semiconductor materials: a case study with terbium (III) and europium (III) in zinc sulfide nanoparticles. J. Phys. Chem. A 115, 4031–4041.
79. Debnath GH, Chakraborty A, Ghatak A, Mandal M, Mukherjee P (2015), Controlled terbium (III) luminescence in zinc sulfide nanoparticles: an assessment of competitive photophysical processes. J. Phys. Chem. C 119, 24132–24141.
80. Manna P, Chakraborty A, Debnath GH, Mukherjee P (2017), How important is the host (semiconductor nanoparticles) identity and absolute band gap in host-sensitized dopant photoluminescence? J. Phys. Chem. Lett. 8, 2794–2798.
81. Debnath GH, Mukherjee P, Waldeck DH (2020), Optimizing the key variables to generate host sensitized lanthanide doped semiconductor nanoparticle luminophores. J. Phys. Chem. C 124, 26495–26517.
82. Bloom BP, Zhao L-B, Wang Y, Waldeck DH, Liu R, Zhang P, Beratan DN (2013), Ligand-induced changes in the characteristic size-dependent electronic energies of CdSe nanocrystals. J. Phys. Chem. C 117, 22401–22411.
83. Hines DA, Kamat PV (2013), Quantum dot surface chemistry: ligand effects and electron transfer reactions. J. Phys. Chem. C 117, 14418–14426.
84. Hines DA, Kamat PV (2014), Recent advances in quantum dot surface chemistry. ACS Appl. Mater. Interfaces 6, 3041–3057.
85. Wu M, Mukherjee P, Lamont DN, Waldeck DH (2010), Electron transfer and fluorescence quenching of nanoparticle assemblies. J. Phys. Chem. C 114, 5751–5759.
86. Chakraborty A, Debnath GH, Ahir M, Bhattacharya S, Upadhyay P, Adhikary A, Mukherjee P (2016), Towards the realization of luminescence from visible emitting trivalent lanthanides (Sm, Eu, Tb, Dy) in polar zinc sulfide nanoparticles: evaluation of *in vitro* cytotoxicity. RSC Adv. 6, 43304–43315.
87. Mukherjee P, Sloan RF, Shade CM, Waldeck DH, Petoud S (2013), A postsynthetic modification of II−VI semiconductor nanoparticles to create Tb^{3+} and Eu^{3+} luminophores J. Phys. Chem. C 117, 14451–14460.
88. Petoud S, Muller G, Moore EG, Xu J, Sokolnicki J, Riehl JP, Le UN, Cohen SM, Raymond KN (2007), Brilliant Sm, Eu, Tb, and Dy chiral lanthanide complexes with strong circularly polarized luminescence. J. Am. Chem. Soc. 129, 77–83.
89. Sudarsan V, van Veggel FCJM, Herring RA, Raudsepp M (2005), Surface Eu^{3+} ions are different than "bulk" Eu^{3+} ions in crystalline doped LaF_3 nanoparticles J. Mater. Chem. 15, 1332–1342.
90. Debnath GH, Rudra S, Bhattacharyya A, Guchhait N, Mukherjee P (2019), Host sensitized lanthanide photoluminescence from post-synthetically modified semiconductor nanoparticles depends on reactant identity. J. Colloid Interface Sci. 540, 448–465.
91. Mehrer H (2007), Diffusion in solids: fundamentals, methods, materials, diffusion-controlled processes, Springer, Berlin,
92. Yin Y, Rioux RM, Erdonmez CK, Hughes S, Somorjai GA, Alivisatos AP (2004), Formation of hollow nanocrystals through the nanoscale Kirkendall effect. Science 304, 711–714.
93. Becker WG, Bard AJ (1983), Photoluminescence and Photoinduced Oxygen Adsorption of Colloidal Zinc Sulfide Dispersions. J. Phys. Chem. 87, 4888–4893.
94. Dunstan DE, Hagfeldt A, Almgren M, Siegbahn HOG, Mukhtar E (1990), Importance of surface reactions in the photochemistry of ZnS colloids. J. Phys. Chem. 94, 6197–6804.
95. Denzler D, Olschewski M, Sattler K (1998), Luminescence studies of localized gap states in colloidal ZnS nanocrystals. J. Appl. Phys. 84, 2841–2845.
96. Dorenbos P, van der Kolk E (2006), Location of lanthanide impurity levels in the III–V semiconductor GaN. Appl. Phys. Lett. 89, 061122-1–061122-3.
97. Dorenbos P (2009), Lanthanide charge transfer energies and related luminescence, charge carrier trapping, and redox phenomena. J. Alloys Compd. 488, 568–573.
98. Chakraborty A, Debnath GH, Saha NR, Chattopadhyay D, Waldeck DH, Mukherjee P (2016), Identifying the correct host−guest combination to sensitize trivalent lanthanide (guest) luminescence: titanium dioxide nanoparticles as a model host system. J. Phys. Chem. C 120, 23870–23882.
99. Carnall WT, Fields PR, Rajnak K (1968), Electronic energy levels in the trivalent lanthanide aquo ions. I. Pr^{3+}, Nd^{3+}, Pm^{3+}, Sm^{3+}, Dy^{3+}, Ho^{3+}, Er^{3+}, and Tm^{3+} J. Chem. Phys. 49, 4424–4442.
100. Carnall WT, Fields PR, Rajnak K (1968), Electronic energy levels of the trivalent lanthanide aquo ions. III. Tb^{3+} J. Chem. Phys. 49, 4447–4449.
101. Carnall WT, Fields PR, Rajnak K (1968), Electronic energy levels of the trivalent lanthanide aquo ions. IV. Eu^{3+} J. Chem. Phys. 49, 4450–4455.
102. Rudra S, Debnath GH, Mukherjee P (2018), Role of reactant concentration and identity of added cation in controlling emission from post-synthetically modified terbium incorporated zinc sulfide nanoparticles: an avenue for the detection of lead(II) cations. RSC Adv. 8, 18093–18108.
103. Zhong X, Feng Y, Knoll W, Han M (2003), Alloyed $Zn_xCd_{1-x}S$ nanocrystals with highly narrow luminescence spectral width. J. Am. Chem. Soc. 125, 13559–13563.
104. Zhong X, Liu S, Zhang Z, Li L, Wei Z, Knoll W (2004), Synthesis of high-quality CdS, ZnS, and $Zn_xCd_{1-x}S$ nanocrystals using metal salts and elemental sulfur. J. Mater. Chem. 14, 2790–2794.
105. Rudra S, Bhar M, Mukherjee P (2019), Structural evolution controls photoluminescence of post-synthetically modified doped semiconductor nanoparticles. J. Phys. Chem. C 123, 29445–29460.
106. Pala IR, Brock SL (2012), ZnS nanoparticle gels for remediation of Pb^{2+} and Hg^{2+} polluted water ACS Appl. Mater. Interfaces 4, 2160–2167.
107. Kurnia F, Hart JN (2015), Band-gap control of zinc sulfide: towards an efficient visible-light-sensitive photocatalyst. ChemPhysChem 16, 2397–2402.
108. Bhar M, Rudra S, Mukherjee P (2020), What role can surface capping ligand play to control dopant emission in semiconductor nanoparticles? J. Phys. Chem. C 124, 6588–6597.
109. Xu S, Wang C, Zhang H, Wang Z, Yang B, Cui Y (2011), pH-Sensitive photoluminescence for aqueous thiol-capped CdTe nanocrystals. Nanotechnology 22, 315703-1–315703-12.

Cite this article as: Rudra S, Bhar M & Mukherjee P 2023. Post-synthetic modification of semiconductor nanoparticles can generate lanthanide luminophores and modulate the electronic properties of preformed nanoparticles. 4open, **6**, 8.